Supplementary Information

A comprehensive quantification of global nitrous oxide sources and sinks

Hanqin Tian[1], Rongting Xu[1], Josep G. Canadell[2], Rona L. Thompson[3], Wilfried Winiwarter[4,5], Parvadha Suntharalingam[6], Eric A. Davidson[7], Philippe Ciais[8], Robert B. Jackson[9,10,11], Greet Janssens-Maenhout[12,13], Michael J. Prather[14], Pierre Regnier[15], Naiqing Pan[1,16], Shufen Pan[1], Glen P. Peters[17], Hao Shi[1], Francesco N. Tubiello[18], Sönke Zaehle[19], Feng Zhou[20], Almut Arneth[21], Gianna Battaglia[22], Sarah Berthet[23], Laurent Bopp[24], Alexander F. Bouwman[25,26,27], Erik T. Buitenhuis[6,28], Jinfeng Chang[8,29], Martyn P. Chipperfield[30,31], Shree R. S. Dangal[32], Edward Dlugokencky[33], James W. Elkins[33], Bradley D. Eyre[34], Bojie Fu[16,35], Bradley Hall[33], Akihiko Ito[36], Fortunat Joos[22], Paul B. Krummel[37], Angela Landolfi[38,39], Goulven G. Laruelle[15], Ronny Lauerwald[8,15,40], Wei Li[8,41], Sebastian Lienert[22], Taylor Maavara[42], Michael MacLeod[43], Dylan B. Millet[44], Stefan Olin[45], Prabir K. Patra[46,47], Ronald G. Prinn[48], Peter A. Raymond[42], Daniel J. Ruiz[14], Guido R. van der Werf[49], Nicolas Vuichard[8], Junjie Wang[27], Ray F. Weiss[50], Kelley C. Wells[44], Chris Wilson[30,31], Jia Yang[51] & Yuanzhi Yao[1]

[1]International Center for Climate and Global Change Research, School of Forestry and Wildlife Sciences, Auburn University, Auburn, AL, USA

[2]Global Carbon Project, CSIRO Oceans and Atmosphere, Canberra, Australian Capital Territory, Australia

[3]Norsk Institutt for Luftforskning, NILU, Kjeller, Norway

[4]International Institute for Applied Systems Analysis, Laxenburg, Austria

[5] Institute of Environmental Engineering, University of Zielona Góra, Zielona Góra, Poland.

[6]School of Environmental Sciences, University of East Anglia, Norwich, UK

[7]Appalachian Laboratory, University of Maryland Center for Environmental Science, Frostburg, MD, USA

[8]Laboratoire des Sciences du Climat et de l'Environnement, LSCE, CEA CNRS, UVSQ UPSACLAY, Gif sur Yvette, France

[9]Department of Earth System Science, Stanford University, Stanford, CA, USA

[10]Woods Institute for the Environment, Stanford University, Stanford, CA, USA

[11]Precourt Institute for Energy, Stanford University, Stanford, CA, USA

[12]European Commission, Joint Research Centre (JRC), Ispra, Italy

[13]Ghent University, Faculty of Engineering and Architecture, Ghent, Belgium

[14]Department of Earth System Science, University of California Irvine, Irvine, CA, USA

[15]Department Geoscience, Environment & Society, Université Libre de Bruxelles, Brussels, Belgium

[16]State Key Laboratory of Urban and Regional Ecology, Research Center for Eco-Environmental Sciences, Chinese Academy of Sciences, Beijing, China

[17]CICERO Center for International Climate Research, Oslo, Norway

[18]Statistics Division, Food and Agriculture Organization of the United Nations, Via Terme di Caracalla, Rome, Italy

[19]Max Planck Institute for Biogeochemistry, Jena, Germany

[20]Sino-France Institute of Earth Systems Science, Laboratory for Earth Surface Processes, College of Urban and Environmental Sciences, Peking University, Beijing, China
[21]Karlsruhe Institute of Technology, Institute of Meteorology and Climate Research/Atmospheric Environmental Research, Garmisch-Partenkirchen, Germany
[22]Climate and Environmental Physics, Physics Institute and Oeschger Centre for Climate Change Research, University of Bern, Bern, Switzerland
[23]Centre National de Recherches Météorologiques (CNRM), Université de Toulouse, Météo-France, CNRS, Toulouse, France
[24]LMD-IPSL, Ecole Normale Supérieure / PSL Université, CNRS; Ecole Polytechnique, Sorbonne Université, Paris, France
[25]PBL Netherlands Environmental Assessment Agency, The Hague, The Netherlands
[26]Department of Earth Sciences – Geochemistry, Faculty of Geosciences, Utrecht University, Utrecht, The Netherlands
[27]Key Laboratory of Marine Chemistry Theory and Technology, Ministry of Education, Ocean University of China, Qingdao, China
[28]Tyndall Centre for Climate Change Research, School of Environmental Sciences, University of East Anglia, Norwich, UK
[29]College of Environmental and Resource Sciences, Zhejiang University, Hangzhou, China.
[30]National Centre for Earth Observation, University of Leeds, Leeds, UK
[31]Institute for Climate and Atmospheric Science, School of Earth and Environment, University of Leeds, Leeds, UK
[32]Woods Hole Research Center, Falmouth, MA, USA
[33]NOAA Global Monitoring Laboratory, Boulder, CO, USA
[34]Centre for Coastal Biogeochemistry, School of Environment Science and Engineering, Southern Cross University, Lismore, New South Wales, Australia
[35]Faculty of Geographical Science, Beijing Normal University, Beijing, China
[36]Center for Global Environmental Research, National Institute for Environmental Studies, Tsukuba, Japan
[37]Climate Science Centre, CSIRO Oceans and Atmosphere, Aspendale, Victoria, Australia
[38] GEOMAR Helmholtz Centre for Ocean Research Kiel, Kiel, Germany
[39]Istituto di Scienze Marine, Consiglio Nazionale delle Ricerche (CNR), Rome, Italy
[40]Université Paris-Saclay, INRAE, AgroParisTech, UMR ECOSYS, Thiverval-Grignon, France
[41]Ministry of Education Key Laboratory for Earth System modeling, Department of Earth System Science, Tsinghua University, Beijing, China
[42]Yale School of Forestry and Environmental Studies, New Haven, CT, USA
[43]Land Economy, Environment & Society, Scotland's Rural College (SRUC), Edinburgh, UK
[44]Department of Soil, Water, and Climate, University of Minnesota, St Paul, MN, USA
[45]Department of Physical Geography and Ecosystem Science, Lund University, Lund, Sweden
[46]Research Institute for Global Change, JAMSTEC, Yokohama, Japan
[47]Center for Environmental Remote Sensing, Chiba University, Chiba, Japan
[48]Center for Global Change Science, Massachusetts Institute of Technology, Cambridge, MA, USA
[49]Faculty of Science, Vrije Universiteit, Amsterdam, Netherlands.
[50] Scripps Institution of Oceanography, University of California San Diego, La Jolla, USA
[51]Department of Forestry, Mississippi State University, Mississippi State, MS, USA

Supporting text

1. Data sources 1
2. Detailed description on multiple approaches 3
2.1 NMIP – Global N_2O Model Inter-comparison Project 3
2.2. The FAOSTAT inventory 5
2.3. The EDGAR v4.3.2 inventory 7
2.4. The GAINS inventory 8
2.5. The SRNM model 9
a. Flux upscaling model 9
b. Global cropland N_2O observation dataset 10
c. Gridded input datasets 11
2.6. Global N flow in aquaculture 11
2.7. Model-based ocean N_2O fluxes 12
2.8. Net N_2O emission from land cover change 13
a. Deforestation area and crop/pasture expansion 13
c. Secondary tropical forest emissions. 14
2.9. Inland water, estuaries, coastal zones 15
a. Riverine N_2O emission simulated by DLEM 15
b. The DLEM estimate on N_2O emission from global reservoirs 16
c. Mechanistic Stochastic Modeling of N_2O emissions from rivers, lakes, reservoirs and estuaries 16
d. Coastal zone emissions 18
2.10. Atmospheric inversion models 18
3. Atmospheric N_2O observations and growth rates for three different atmospheric networks (NOAA, AGAGE, and CISRO) 21
4. Comparison with the IPCC AR5 23
5. Per capita N_2O emission at global and regional scales in the recent decade 24

Supporting tables

Supplementary Table 1 N_2O emissions from global agricultural soils based on multiple bottom-up approaches including the additions of mineral N fertilizer, manure and crop residues, and cultivation of organic soils. 32

Supplementary Table 2 N_2O emissions from global total area under permanent meadows and pasture, due to manure N deposition (left on pasture) based on EDGAR v4.3.2, FAOSTAT, and GAINS estimates. 32

Supplementary Table 3 N_2O emissions due to global manure management based on multiple bottom-up approaches. 33

Supplementary Table 4 Aquaculture N_2O emissions based on multiple sources. 33

Supplementary Table 5 Anthropogenic N_2O emissions from the global inland waters based on process-based models 34

Supplementary Table 6 Anthropogenic N_2O emissions from the global inland waters based on multiple bottom-up approaches 34

Supplementary Table 7 Natural N_2O emissions from the global inland waters based on process-based models. 35

Supplementary Table 8 Nitrous oxide emissions due to atmospheric N deposition on land based on multiple bottom-up approaches 35

Supplementary Table 9 Global N_2O emissions from waste and waste water based on EDGAR v4.3.2 and GAINS estimates. 36

Supplementary Table 10 Global N_2O emissions from fossil fuel and industry based on multiple bottom-up approaches. 36

Supplementary Table 11 Global N_2O emissions from biomass burning based on multiple bottom-up approaches 37

Supplementary Table 12 Global oceanic N_2O emissions based on multiple models. 37

Supplementary Table 13 Global N_2O emissions based on multiple top-down approaches. 38

Supplementary Table 14 Comparison of terminologies used in this study and previous reports. .39

Supplementary Table 15 Comparison of the global N_2O budget in this study with the IPCC AR5. 40

Supplementary Table 16 Simulation experiments in the NMIP (Tian et al.[1,17]) 41

Supplementary Table 17 Information of NMIP models using in this study 41

Supplementary Table 18 Summary of models in ocean N_2O inter-comparison 42

Supplementary Table 19 Overview of the inversion frameworks that are included in the global N_2O budget 42

Supporting figures

Supplementary Fig. 1 Spatial distribution of ten study regions across the globe. 43
Supplementary Fig. 2 Per capita N_2O emission (kg N capita^{-1} yr^{-1}) during 2007–2016. 44

1. Data sources

Bottom-up methods include process-based models (NMIP[1] including six process-based terrestrial biosphere models, DLEM-only[2] for pastureland, five ocean models[3-8], one mechanistic stochastic model[9,10]), four GHG emission databases [EDGAR v4.3.2[11], FAOSTAT[12], GAINS[13], GFED4s[14] (only for biomass burning), and one statistical model (SRNM) only for cropland soils[15]. The top-down approach includes four independent atmospheric inversion frameworks[16]. The NMIP result provides nitrous oxide (N_2O) emissions from natural and agricultural soils, defined as soils in agricultural land, during 1860–2016, with consideration of multiple environmental factors, such as climate, elevated atmospheric carbon dioxide (CO_2), land cover and land use change, atmospheric nitrogen (N) deposition, mineral N fertilizer, and manure N in cropland[17]. Mineral N fertilizer and manure N are mainly applied to cropland, while N deposition can reach soils under all land uses. Natural soil emissions were estimated by NMIP based on the ensemble mean of six models (Supplementary Table 16): (1) the Dynamic Land Ecosystem Model (DLEM)[18,19], (2) Land Processes and eXchanges model - Bern (LPX-Bern v1.4)[20,21], (3) O-CN[22], (4) Organising Carbon and Hydrology In Dynamic Ecosystems (ORCHIDEE)[23], (5) Organising Carbon and Hydrology In Dynamic Ecosystems-Carbon Nitrogen Phosphorus (ORCHIDEE-CNP)[23], and (6) Vegetation Integrated SImulator for Trace gases (VISIT)[24,25] (See more model information in Tian et al.[1,17]). Agricultural soil emissions were from manure and fertilizer N applications on cropland during 1860–2016[1] and intensively managed grassland (pastures) during 1900–2014[2]. For 'Indirect emissions from anthropogenic N additions', we considered emissions from atmospheric N deposition and 'Inland and coastal waters' N leaching/runoff including five sub-systems: rivers, lakes, estuaries, reservoirs, and coastal zones. Yao et al.[26] estimated N_2O emissions from rivers using the process-based model (DLEM) during 1900–2016 and provided estimates from reservoirs as well, while emissions determined from the stochastic mechanistic model of Maavara et al.[10] and Lauerwald et al.[9] for the river-reservoir-estuary continuum, and lakes, respectively, were in 2000. Coastal zone emissions were obtained from data compilation reported in Camillini et al.[27] and Murray et al.[28]. The DLEM model also provided an estimate of N_2O emissions from biomass burning across various biomes (crop residue and savannas, peatland, tropical forest, temperate forest, and boreal forest) during 1860–2015. A nutrient budget model for shellfish and finfish[29-31] was used to calculate the nutrient flows in aquaculture

production systems. For computing the N_2O emission we consider the amount of N released to the environment, i.e. the difference between N intake and N in the harvested fish, which includes all the nutrient excretion. Estimates of oceanic N_2O fluxes are derived from an inter-comparison of five global ocean biogeochemistry models including Bern-3D[3], NEMOv3.6-PISCESv2-gas[4], NEMO-PlankTOM10[5], UVic2.9[6], and NEMO-PISCES 3.2[7].

The EDGAR v4.3.2 applies the IPCC guidelines mostly at Tier-1, but integrates higher tier information based on available country reporting, mostly from Annex I countries. It provided data from 1970 to 2012. We updated the data to 2016 based on the global and regional trends between 2000 and 2012 for each individual category. In EDGAR v4.3.2, 'Indirect emission from N deposition' only represents non-agricultural activities. 'Waste and waste water' includes 'Waste incineration' and 'Wastewater handling'. We merged 'Transportation', 'Energy', 'Industry', and 'Residential and other sectors' to represent the total emission from 'Fossil fuel and industry'. Since the EDGAR v4.3.2 database did not provide the emission of 'Biomass burning' from land use outside of agriculture, here we did not include its estimate of 'Agriculture waste burning' into the data synthesis. The FAOSTAT emissions database of the Food and Agriculture Organization of the United Nations (FAO) covers emissions of N_2O from agriculture and land use by country and globally, from 1961 to 2017 for agriculture, and from 1990[12] for relevant land use categories, i.e, cultivation of histosols, biomass burning, etc., applying only Tier-1 coefficients[32]. In addition to the IPCC agriculture burning categories 'Burning crop residues' and 'Burning savannah', FAOSTAT also estimates N_2O emissions from deforestation fires, forest fires and peatland fires. Emissions from 'Fossil fuel and industry' are directly adapted from the EDGAR v4.3.2 emission inventory. The GAINS model[13] provided N_2O emissions data every five-years (i.e., 1990, 1995, 2000, 2005, 2010, 2015). We assumed the change between each five-year estimate was linear. To avoid abrupt jumps between 1989 and 1990 during data synthesis, we linearly extrapolated data to 1980 through using estimates in 1990 and 1995 in each sub-sector. 'Direct soil emissions' are from synthetic N fertilizer, animal manure, cultivation of histosols, and crop residues. 'Indirect emissions from anthropogenic N additions' are from 'N deposition on land' and 'Inland and coastal waters' (i.e., lakes, rivers, and shelf seas). The source of 'N deposition on land' is mainly from agricultural activities, but it deposited on all global ice-free areas (i.e., agricultural land, forest land, other land uses). The 'Energy' emission includes conversion, industry, transport, and domestic. The 'Industry'

emission includes nitric acid plants, adipic acid plants, and caprolactam plants. We merged 'Energy' and 'Industry' to represent 'Fossil fuel and industry' emissions. They also considered N_2O use, but we did not include this sector in the synthesis table. We merged 'Composting' and 'Wastewater' sectors into 'Waste and waste water' to make comparison with the EDGAR v4.3.2 database. In addition, the sector 'Grazing' was treated as 'Manure left on pasture' to make comparison. The GFED4s emission inventory[14] provided N_2O emissions from 'Biomass burning' including agricultural waste and other biomass burning (i.e., Savanna, grassland, and shrubland fires, boreal forest fires, temperate forest fires, deforestation and degradation, and peatland fires) during 1997–2016.

The spatially-referenced non-linear model SRNM was fitted through considering environmental factors and N management practices to generate gridded annual EF maps at 5′ spatial resolution, and then to calculate global/regional N_2O emissions during 1901–2016 together with time-series N input datasets[15]. This database provides N_2O emissions from global and regional cropland with the application of synthetic N fertilizer and manure N for the period 1980–2016.

For the top-down constraints on the global and regional N_2O emissions for the period 1998–2016, we have used estimates from four independent atmospheric inversion frameworks (INVICAT, PyVAR, MIROC4-ACTM, and GEOSChem), all of which used the Bayesian inversion method. Here, two versions of PyVAR were run using different ocean priors (one high and one low) for determining the sensitivity to the ocean prior. These runs are denoted as PyVAR-1 and PyVAR-2, respectively. For the top-down global estimate, we used the original spatial resolution in each framework. For the top-down regional estimate, we interpolated the coarse resolution into 1° × 1° to cover all land areas in the four frameworks (see details in section 2.10).

2. Detailed description on multiple approaches

2.1 NMIP – Global N_2O Model Inter-comparison Project

Ten process-based Terrestrial Biosphere Models (TBMs) participate in NMIP. In general, N_2O emissions from soil are regulated at two levels, which are the rates of nitrification and denitrification in the soil and soil physical factors regulating the ratio of N_2O to other nitrous

gases[33]. For N input to land ecosystems, all ten models considered the atmospheric N deposition and biological fixation, nine models with crop N_2O module included N fertilizer use, but only six models considered manure as N input. For vegetation processes, all models included dynamic algorithms in simulating N allocation to different living tissues and vegetation N turnover, and simulated plant N uptake using the "Demand and Supply-driven" approach. For soil N processes, all ten models simulated N leaching according to water runoff rate; however, models are different in representing nitrification and denitrification processes and the impacts of soil chemical and physical factors. The differences in simulating nitrification and denitrification processes are one of the major uncertainties in estimating N_2O emissions. Algorithms associated with N_2O emissions in each participating model are briefly described in Appendix A of Tian et al.[17].

All participating models are driven by consistent input datasets (i.e., climate, atmospheric CO_2 concentration, land cover change, atmospheric N deposition, mineral N fertilization, and manure N application) and implemented seven simulation experiments (SE0 – SE6; Supplementary Table 17) at the spatial resolution of 0.5° globally covering the period of 1861–2016 (ref. [1]). The SE1 includes all driving factors for models with manure addition, and the SE2 is the experiment including all the driving factors for models except manure N. In the SE0 simulation, driving forces were kept constant at the level in 1860 over the entire simulation period (1861–2016).

By comparing results from different model scenarios, it is possible to attribute the changed spatiotemporal variations of soil N_2O emissions to the variations of six natural and anthropogenic factors, namely, climate (CLIM, including precipitation, humidity, temperature and photosynthetic active radiation changes), atmospheric CO_2 concentration (CO_2), land cover change (LCC), atmospheric N deposition (NDEP), mineral N fertilizer use (NFER), and manure N use in cropland (MANN). In order to understand soil N_2O emissions dynamics caused by crop cultivation, we further separated the global and regional N_2O emissions into those derived from cropland soils and those from soils of other land ecosystems. All soils in other land ecosystems except cropland were treated as "natural soils" while model simulations were implemented in this study. Except for cropland, the current NMIP simulations do not include management

practices (such as grazing and forest logging) for other managed ecosystems such as pasture, planted forests and urban.

In this study, we aimed to attribute the impact of single factor on cropland N_2O emissions, thus participating models without providing SE2–SE6 and SE0 results in cropland were excluded. Here, we included estimates from six process-based models (Supplementary Table 16). Four models (DLEM, ORCHIDEE, ORCHIDEE-CNP, and VISIT) considered the effects of manure N application in cropland and ran all the seven simulation experiments (SE0–SE6), while the other two models (LPX-Bern and O-CN) did not include manure effects and ran six model experiments (all except SE1). We used four model results (i.e., DLEM, ORCHIDEE, ORCHIDEE-CNP, and VISIT) to calculate the manure N effect (SE1–SE2). Meanwhile, we used six model results (i.e., DLEM, LPX-Bern, O-CN, ORCHIDEE, ORCHIDEE-CNP, and VISIT) to calculate the effects of synthetic N fertilizer use (SE2–SE3) and atmospheric N deposition (SE3–SE4). The effect of N deposition in natural vegetation was calculated from the six models mentioned above.

2.2. The FAOSTAT inventory

The FAOSTAT emissions data are computed at Tier 1 following IPCC, 2006, Vol. 4. The overall equation is as follows:

Direct emissions are estimated at country level, using the formula:

$$Emission = A * EF \quad (1a)$$

where emission represents kg N yr^{-1}; A represents amount of N in the following items (annual synthetic N applications/manure applied to soils/manure left on pasture/manure treated in manure management systems/crop residue/biomass burned amount) in kg N yr^{-1}; EF = Tier 1, default IPCC emission factors, expressed in kg N/kg N.

Indirect emissions are estimated at country level, using the formula:

$$Emission = A_{v\&l} * EF \quad (1b)$$

where emission represents kg N yr^{-1}; $A_{v\&l}$ represents the fraction of manure/synthetic N fertilizers that volatize as NH_3 and NO_x and are lost through runoff and leaching in kg N yr^{-1}; *EF* = Tier 1, default IPCC emission factors, expressed in kg N/kg N.

Synthetic N fertilizers: N_2O from synthetic fertilizers is produced by microbial processes of nitrification and denitrification taking place on the addition site (direct emissions), and after volatilization/redeposition and leaching processes (indirect emissions).

Manure management: The term manure includes both urine and dung (i.e., both liquid and solid material) produced by livestock. N_2O is produced directly by nitrification and denitrification processes in the manure, and indirectly by N volatilization and redeposition processes.

Manure applied to soils: N_2O is produced by microbial processes of nitrification and denitrification taking place on the application site (direct emissions), and after volatilization/redeposition and leaching processes (indirect emissions).

Manure left on pastures: N_2O is produced by microbial processes of nitrification and denitrification taking place on the deposition site (direct emissions), and after volatilization/redeposition and leaching processes (indirect emissions).

Crop Residue: N_2O emissions from crop residues consist of direct and indirect emissions from N in crop residues left on agricultural fields by farmers and from forages during pasture renewal (following the definitions in the IPCC guidelines[34]). Specifically, N_2O is produced by microbial processes of nitrification and denitrification taking place on the deposition site (direct emissions), and leaching processes (indirect emissions).

Cultivation of organic soils: The FAOSTAT domain “Cultivation of organic soils” contains estimates of direct N_2O emissions associated with the drainage of organic soils – histosols – under cropland and grazed grassland.

Burning-savanna: N_2O emissions from the burning of vegetation biomass in the land cover types: Savanna, Woody Savanna, Open Shrublands, Closed Shrublands, and Grasslands. Burning-crop residues: N_2O produced by the combustion of a percentage of crop residues burnt on-site. Burning-biomass: N_2O emissions from the burning of vegetation biomass in the land cover types: Humid tropical forest, other forest, and organic soils.

2.3. The EDGAR v4.3.2 inventory

The new online version, EDGAR v4.3.2 incorporates a full differentiation of emission processes with technology-specific emission factors and additional end-of-pipe abatement measures6 and as such updates and refines the emission estimates. The emissions are modelled based on latest scientific knowledge, available global statistics, and methods recommended by IPCC (2006)[34]. Official data submitted by the Annex I countries to the United Nations Framework Convention on Climate Change (UNFCCC) and to the Kyoto Protocol are used to some extent, particularly regarding control measures implemented since 1990 that are not described by international statistics.

The N_2O emission factor for direct soil emissions of N_2O from the use of synthetic fertilizers and from manure used as fertilizers and from crop residues is taken from IPCC (2006)[34], that updated the default IPCC emission factor in the IPCC Good Practice Guidance (2000) with a 20% lower value. N_2O emissions from the use of animal waste as fertilizer are estimated taking into account both the loss of N that occurs from manure management systems before manure is applied to soils and the additional N introduced by bedding material. N_2O emissions from fertilizer use and CO_2 from urea fertilization are estimated based on IFA and FAO statistics.

N_2O emissions from manure management are based on distribution of manure management systems from Annex I countries reporting to the UNFCCC, Zhou et al.[35] for China and IPCC (2006)[34] for the rest of the countries.

Different N_2O emission factors are applied to tropical and non-tropical regions. N and dry matter content of agricultural residues are estimated from the cultivation area and yield for 24 crop types (two types of beans, barley, cassava, cereals, three types of peas, lentils, maize, millet, oats, two types of potatoes, pulses, roots and tubers, rice, rye, soybeans, sugar beet, sugar cane, sorghum, wheat and yams) from FAOSTAT (2014) and using emission factors of IPCC (2006)[34].

Indirect N_2O emissions from leaching and runoff of nitrate are estimated from N input to agricultural soils as described above. Leaching and runoff are assumed to occur in all agricultural areas except non-irrigated dryland regions, which are identified with maps of FAO Geonetwork (2011). The fraction of N lost through leaching and runoff is based on the study of Van Drecht et al.[36]. The updated emission factor for indirect N_2O emissions from N leaching and run-off from

the IPCC (2006) guidelines is selected, while noting that it is 70% lower than the mean value of the 1996 IPCC Guidelines and the IPCC Good Practice Guidance (IPCC, 1997, 2000).

Indirect N_2O emissions from atmospheric deposition of N of NO_x and NH_3 emissions from non-agricultural sources, mainly fossil fuel combustion, are estimated using N in NO_x and NH_3 emissions from these sources as activity data, based on EDGAR v4.3.2 database for these gases. The same emission factor from IPCC (2006)[34] is used for indirect N_2O from atmospheric deposition of N from NH_3 and NOx emissions, as for agricultural emissions.

2.4. The GAINS inventory

The methodology adopted for the estimation of current and future greenhouse gas emissions and the available potential for emission controls follows the standard methodology used by the Greenhouse Gas - Air Pollution Interactions and Synergies (GAINS) model[37]. For a given year, emissions of each pollutant *p* are calculated as the product of the activity levels, the "uncontrolled" emission factor in the absence of any emission control measures, the efficiency of emission control measures and the application rate of such measures:

$$E_{i,p} = \sum_{j,a,t} E_{i,j,a,t,p} = \sum_{j,a,t} A_{i,j,a} ef_{i,j,a,p} (1 - eff_{t,p}) X_{i,j,a,t} \quad (2)$$

where subscripts *i,j,a,t,p* denote region, sector, activity, abatement technology, and pollutant, respectively; *Ei,p* represents emissions of the specific pollutant *p* in region *i; Aj* represents activity in a given sector *j; ef* represents "uncontrolled" emission factor; *eff* represents reduction efficiency; *X* represents actual implementation rate of the considered abatement.

Results (emissions from all anthropogenic sources) are available in 5-year intervals from 1990 to 2050 (in some regions up to 2070) for each GAINS region, typically comprising one country to express areas of common legislation also with respect of air pollution. Very large countries have been further split along administrative areas, while in cases of limited data availability also groups of countries have been combined into GAINS regions.

For N_2O, the fate of emissions abatement is often connected with action taken to control other pollutants. For example, it may occur that after control (e.g., of NO_x emissions), N_2O emissions become higher than in the unabated case. To reflect this effect, negative reduction efficiencies would need to be used for N_2O. As it is difficult to communicate such negative numbers, GAINS

has resorted to present "controlled" emission factors instead, which describe the emission factor of a process after installation of abatement technology.

2.5. The SRNM model

a. Flux upscaling model

The SRNM model[38] was applied to simulate direct cropland-N_2O emissions. In SRNM, N_2O emissions were simulated from N application rates using a quadratic relationship, with spatially-variable model parameters that depend on climate, soil properties, and management practices. The original version of SRNM was calibrated using field observations from China only[39]. In this study, we used the global N_2O observation dataset to train it to create maps of gridded annual emission factors of N_2O and the associated emissions at 5-minute resolution from 1901 to 2014[15]. The gridded EF and associated direct cropland-N_2O emissions are simulated based on the following equation:

$$E_{ijt} = \alpha_{ij} N_{ijt}^2 + \beta_{ij} N_{ijt} + \varepsilon_{ijt}, \ \forall i \tag{3a}$$

where

$$\alpha_{ij} \sim N\left(\sum_k \left(x_k \lambda_{ijk}\right), \sigma_{ijk}^2\right), \ \beta_{ij} \sim N\left(\sum_k \left(x_k \phi_{ijk}\right), \sigma_{ijk}'^2\right) \tag{3b}$$

$$\lambda_{ijk} \sim N\left(\mu_{ijk}, \omega_{ijk}^2\right), \ \phi_{ijk} \sim N\left(\mu_{ijk}', \omega_{ijk}'^2\right), \ \varepsilon_{ijt} \sim N\left(0, \tau^2\right) \tag{3c}$$

and i denotes the sub-function of N_2O emission (i=1, 2, …, I) that applies for a sub-domain division Ω_i of six climate or soil factors, j represents the type of crop (j=1-2, 1 for upland crops and 2 for paddy rice), k is the index of climate or soil factors (k=1-6, i.e., soil pH, clay content, soil organic carbon, bulk density, the sum of cumulative precipitation and irrigation, mean daily air temperature). Ω_i denotes a set of the range of multiple x_k. E_{ijt} denotes direct N_2O emission flux (kg N ha^{-1} yr^{-1}) estimated for crop type j in year t in the ith sub-domain, N_{ijt} is N application rate (kg N ha^{-1} yr^{-1}), and α_{ij} and β_{ij} are defined as summation of the product of x_k and λ_{ijk} over k. The random terms λ and ϕ are assumed to be independent and normally distributed, representing

the sensitivity of α and β to x_k. ε is the model error. μ and μ' are the mean effect of x_k for α and β, respectively. σ, σ', ω, ω', and τ are standard deviations. Optimal sub-domain division, associated parameters mean values and standard deviations were determined by using the Bayesian Recursive Regression Tree version 2 (BRRT v2)[39-41], constrained by the extended global cropland-N_2O observation dataset. The detailed methodological approach of the BRRT v2 is described in Zhou et al.[41]

b. Global cropland N_2O observation dataset

We aggregated cropland N_2O flux observation data from 180 globally distributed observation sites from online databases, on-going observation networks, and peer-reviewed publications. Chamber-based observations were only included in this dataset. These data repositories are as follows: the NitroEurope, CarbonEurope, GHG-Europe (EU-FP7), GRACEnet, TRAGnet, NANORP, and 14 meta-analysis datasets[42-55]. Four types of data were excluded from our analysis: (i) observations without a zero-N control for background N_2O emission, (ii) observations from sites that used controlled-release fertilizers or nitrification inhibitors, (iii) observations not covering the entire crop growing season, (iv) observations made in laboratory or greenhouse. We then calculated cropland-N_2O emissions as the difference between observed N_2O emission (E) and background N_2O emission (E_0). Values of EF were estimated for each nonzero N application rate (N_a) as direct cropland-N_2O emission divided by N_a: $EF = (E - E_0)/N_a$. This yielded a global dataset of direct cropland-N_2O emissions, N-rate-dependent N_2O EFs and fertilization records from each site (i.e., 1,052 estimates for upland crops from 152 sites and 154 estimates for paddy rice from 28 sites), along with site-level information on climate, soils, crop type, and relevant experimental parameters. Total numbers of sites and total measurements in the dataset were more than doubled those for previous datasets of N_2O EF. The extended global N_2O observation network covered most of fertilized croplands, representing a wide range of environmental conditions globally. For each site in our dataset, the variables included four broad categories: N_2O emissions data, climate data (cumulative precipitation and mean daily air temperature), soil attributes (soil pH, clay content, SOC, BD), and management-related or experimental parameters (N application rate, crop type). More details on global cropland N_2O observation dataset can be found in Wang et al.[15]

c. Gridded input datasets

The updated SRNM model was driven by many input datasets, including climate, soil properties, N inputs (e.g., synthetic N fertilizer, livestock manure and crop residues applied to cropland), as well as the historical distribution of cropland. Cumulative precipitation and mean daily air temperature over the growing season were acquired from the CRU TS v3.23 climate dataset[43] (0.5-degree resolution), where growing season in each grid cell was identified following Sacks et al.[52] The patterns of SOC, clay content, BD, and soil pH were acquired from the HWSD v1.2 (ref.[56], 1-km resolution). Both climate and soil properties were re-gridded at a resolution of 5′ × 5′ using a first-order conservative interpolation widely used in the CMIP5 model intercomparison[57]. Annual cropland area at 5′ spatial resolution from 1901 to 2014 was obtained from the History Database of the Global Environment (HYDE 3.2.1)[58]. N inputs of synthetic fertilizers were generated based on sub-national statistics (i.e., county-, municipal, provincial or state-levels) of N-fertilizer consumption of 15,593 administrative units from 38 national statistical agencies and national statistics of the other 197 countries from FAOSTAT. N inputs of livestock manure and crop residues applied to cropland were provided by Zhang et al.[59] and FAOSTAT, respectively. To compute crop-specific N application rates, we allocated N inputs for upland crops and paddy rice based on the breakdown (or proportion) of total fertilizer use by crop from Rosas[60]. Crop-specific N application rates (N_{ijt}) were finally resampled into grid maps at 5′ spatial resolution following the dynamic cropland distributions of the HYDE 3.2.1. The assumption of a maximum combined synthetic + manure + crop residues N application rate was 1,000 kg N ha^{-1}, larger than the previous threshold[61] that was only applied for the sum of synthetic fertilizers and manure.

2.6. Global N flow in aquaculture

We apply a nutrient budget model for shellfish and finfish[62-64] to calculate the nutrient flows in aquaculture production systems. These flows comprise feed inputs, retention in the fish, and nutrient excretion. Individual species within crustaceans, seaweed, fish and molluscs are aggregated to the International Standard Statistical Classification of Aquatic Animals and Plants (ISSCAAP) groups[65], for which production characteristics are specified. Feed and nutrient conversion rates are used for each ISSCAAP group to calculate the feed and nutrient intake from

production data from FAO[65]. Feed types include home-made aquafeeds and commercial compound feeds with different feed conversion ratios that also vary in time due to efficiency improvement; in addition, the model accounts for algae in ponds, that are often fertilized with commercial fertilizers or animal manure, consumed by omnivore fish species like carp. A special case is the filter-feeding bivalves that filter seston from the water column, and excrete pseudofeces, feces and dissolved nutrients. Based on production data and tissue/shell nutrient contents the model computes the nutrient retention in the fish. Using apparent digestibility coefficients, the model calculates outflows in the form of feces (i.e. particulate nutrients) and dissolved nutrients. Finally, nutrient deposition in pond systems and recycling is calculated. For computing the N_2O emission we consider the amount of N released to the environment, i.e. the difference between N intake and N in the harvested fish, which includes all the nutrient excretion. Since in pond cultures part of that N is managed, we made the amount of N recycling explicit, as well as ammonia emissions from ponds. This is to avoid double counting when computing N_2O emissions from crop production.

2.7. Model-based ocean N_2O fluxes

Oceanic N_2O is produced by microbial activity during organic matter cycling in the subsurface ocean; its production mechanisms display significant sensitivity to ambient oxygen level. In the oxic ocean, N_2O is produced as a byproduct during the oxidation of ammonia to nitrate, mediated by ammonia oxidizing bacteria and archaea. N_2O is also produced and consumed in sub-oxic and anoxic waters through the action of marine denitrifiers during the multi-step reduction of nitrate to gaseous N. The oceanic N_2O distribution therefore displays significant heterogeneity with background levels of 10-20 nmol/l in the well-oxygenated ocean basins, high concentrations (> 40 nmol/l) in hypoxic waters, and N_2O depletion in the core of ocean oxygen minimum zones (OMZs).

Oceanic N_2O emissions are estimated to account for up to a third of the pre-industrial N_2O fluxes to the atmosphere, however, the natural cycle of ocean N_2O has been perturbed in recent decades by inputs of anthropogenically derived nutrient (via atmospheric deposition and riverine fluxes), and by the impacts of climate change (via impacts on biological productivity and ocean deoxygenation).

Estimates of oceanic N_2O fluxes for the Global N_2O Budget synthesis are derived from an inter-comparison of five global ocean biogeochemistry models that include explicit representation of the oceanic N_2O cycle (Supplementary Table 18). Ocean biogeochemistry models include process representation of ocean circulation, nutrient cycling and trace-gas generation. In particular, the N_2O fluxes to the atmosphere are derived from N_2O cycle parameterizations embedded in the ocean biogeochemistry models and combined with a parameterization of gas-exchange across the air-sea interface. The models participating in this inter-comparison are taken from the recent studies of Battaglia and Joos[3], Berthet et al.[4], Buitenhuis et al.[5], Landolfi et al.[6], and Martinez-Rey et al.[7].

The models differ in aspects of physical configuration (e.g., spatial resolution), meteorological forcing applied at the ocean surface, and in their parameterizations of ocean biogeochemistry; specific details on individual models are provided in the publications listed in Supplementary Table 18. Towards the N_2O budget synthesis, all modelling groups reported annual mean estimates of ocean-atmosphere N_2O fluxes for the period 1980–2016 (or for as many years as possible in that period). Fluxes were reported at the following spatial scales: (a) global; (b) Southern latitudes (90°–30°S); (c) Tropics (30°S–30°N); and (d) Northern latitudes (30°–90°N). In addition, four modelling groups reported annually averaged ocean N_2O fluxes at higher spatial resolution; i.e., gridded to a $1^o \times 1^o$ resolution.

2.8. Net N_2O emission from land cover change

a. Deforestation area and crop/pasture expansion

Two sets of deforestation area were used to represent land cover changes during 1860–2016. The LUH2 v2h (land use harmonization, http://luh.umd.edu) land use forcing data were used to derive the deforestation area and its partition between crops and pastures from 1860–2016. LUH2 categorizes forest lands into forested primary land and potentially forested secondary land, while croplands are divided into C3 annual crops, C3 perennial crops, C4 annual crops, C4 perennial crops, and C3 N-fixing crops. In the empirical computation, all sub-classes within each land use type were treated the same. Thus only the annual transition area from forests to croplands or managed pasture was needed.

In the process-based estimates, the model requires input of the plant functional types (PFTs) of the forests (e.g., tropical broadleaf evergreen forest and tropical broadleaf deciduous forest), and the species of croplands (e.g., wheat and rice). Thus, a potential vegetation map and the accompanied composition ratio map of each natural PFT acquired from the Synergetic Land Cover Product (SYNMAP) were jointly used with LUH2 v2h to generate the historical spatial distribution of PFTs.

b. Methods

Here we ran the DLEM model with varying climate and CO_2 but hold other factors constant to estimate forest baseline emissions and unfertilized crop/pasture emissions from 1860-2016. The climate data were acquired from CRU-NCEP v7 (https://vesg.ipsl.upmc.fr), which is a fusion of the CRU and NCEP/NCAR reanalysis products at a spatial resolution of 0.5° × 0.5° and a daily time-step. The atmospheric CO_2 data were obtained from NOAA GLOBLVIEW-CO2 dataset (https://www.esrl.noaa.gov), which are derived from atmospheric and ice core measurements. In the tropical area, both estimates from the DLEM model and the bookkeeping method were adopted, whereas in extra-tropical area, we only adopted the DLEM outputs.

c. Secondary tropical forest emissions

There are not many published studies on N_2O emissions from secondary tropical forests that grow back after crop or pasture abandonment. A recent meta-analysis by Sullivan et al.[66] lumps together all forms of N "gas loss" including NO and N_2O, so it does not address N_2O specifically. It also reviews the data for secondary forests across the tropics and shows that eight N cycling parameters, including N gas loss and some other parameters that overlap with those measured by Davidson et al.[67] and Keller and Reiners[68], recover only gradually during secondary tropical forest succession. Their meta-analysis of the N gas loss parameter showed a significant positive slope, indicating gradually increasing gas loss rates with age after initiation of secondary forest regrowth[66]. Keller and Reiners[68] showed a gradual recovery of soil nitrate and soil emissions of N_2O and nitric oxide (NO) during 20 years of secondary forest succession. As shown, N_2O emissions did not return to the level of the primary forest after about 20 years of secondary forest succession. Davidson et al.[67] found that it takes 40–70 years of secondary forest succession for N_2O emissions to approach levels of the primary forest. This is also consistent with other trends of related N cycling parameters, such as the nitrate:ammonium ratio, soil

nitrate, litter mass:N, litterfall N:P, and foliar ^{15}N. In this study, through using the sites of field observation from Davidson et al.[67] and Keller and Reiners[68], we estimated N_2O emission from secondary tropical forests based on the algorithm: y=0.0084x + 0.2401 (R^2 = 0.44).). x (unit: year) indicates secondary forest age and y (unitless; 0−1) indicates the ratio of secondary forest N_2O emission over that of a reference mature forest. The difference between primary forests and secondary forests were subtracted from natural soil emissions simulated by six land-surface models in NMIP.

2.9. Inland water, estuaries, coastal zones

a. Riverine N_2O emission simulated by DLEM

Here we developed a riverine N_2O module within a scale adaptive water transport model and coupled with the DLEM model[15]. The land surface module of DLEM-simulated N species (NO_3^-, NH_4^+, DON and PON) leaching from soils when N inputs were into the water transport model. The river routine module within the DLEM is a fully distributed water transport model, which explicitly calculated the flow routine cell-to-cell based on hydraulics methods. The water quality module built into the water transport module can simulate the carbon lateral transportation, biogeochemical reactions (e.g., decomposition of organic matter, nitrification, denitrification), CO_2 degassing and physical deposition of particle organic matter and has been successfully applied in the Gulf of Mexico and the U.S. east coast[69-75]. Specifically, by introducing sub-grid routine processes technology into the model, the scale adaptive water transport module can effectively address the physical and biogeochemical processes of the small streams within a grid cell, which has been overly simplified in earth system models. We validated global N fluxes based on GEMS-GLORI world river discharge database. The newly developed riverine N_2O module receives dissolved N_2O from land and groundwater, atmosphere wet deposition, and calculate the dynamics of dissolved N_2O concentration and fluxes in both small streams and large rivers. Here, we validated the annual mean riverine N_2O concentration, ground water N_2O concentration, and riverine N_2O emissions globally based on literature survey. DLEM simulated results all agree well with the observations.

b. The DLEM estimate on N_2O emission from global reservoirs

We assumed the reservoirs were linked to rivers, and thus these aquatic systems shared the similar N_2O emission rates in the large-scale studies. We therefore estimate the reservoir surface-area form the Global Reservoirs and Dams (GRanD) database. In riverine N_2O fluxes estimations, we have two N_2O fluxes rates: one is the emission from the large river channel, and the other one is the emission from small rivers within the grid cell. We obtained the upstream area of each dam from the GRanD database and overlaid with the area raster of the 0.5° cell. If the upstream area of a dam is less than the area of its belonging 0.5° grid cell, we considered the dam was located at the small streams within the grid cell and the fluxes of that dam equal to the small river N_2O fluxes of that grid. On the contrary, if the upstream area was larger than the area of the grid cell, the dam is located at the large river channel, thus the fluxes of that dam equal to the riverine N_2O fluxes of the main channel in that grid cell. Align with uncertainty analysis in the riverine N_2O estimations, we overlaid the surface area of dams with riverine N_2O emission rate estimates from the nine-uncertainty experiments to get the reservoir N_2O emissions. We calculated the average as the final reported value.

c. Mechanistic Stochastic Modeling of N_2O emissions from rivers, lakes, reservoirs and estuaries

In our calculations, we used a process-oriented model recently developed to estimate N_2O emissions from inland waters, including rivers, reservoirs and estuaries[10]. To estimate N_2O emissions from lakes[9], we applied the same approach to a global lake dataset[76]. Based on a spatially explicit representation of water bodies and point and non-point sources of N and phosphorus (P), this model quantifies the global scale spatial patterns in inland water N_2O emissions in a consistent manner at 0.5° resolution. The methodology is based on the application of a stochastic Monte Carlo-based model to estimate average annual rates of primary production, ammonification, nitrification, denitrification, N fixation and burial of N in sediments as well as N_2O production and emission generated by nitrification and denitrification. Because of the scarcity of observations, the Monte Carlo approach is a necessary step to generate predictive equations for the N budget and N_2O emission of each inland water body based on inputs of total N (TN) and total P (TP) from the watershed and water residence times in a given river segment, lake, reservoir or estuary[9,10]. In situ N cycling processes for each specific water body worldwide cannot be predicted due to the lack of parameter constraints or data at this fine granularity.

Instead, the model is fed with hypothetical but realistic combinations of physical and biogeochemical parameters through the use of probability density functions (PDFs) approximating the global statistical distribution of those parameters as derived from literature values and databases. A Monte Carlo analysis of the model is then performed, in which parameters are stochastically selected from the pre-assigned PDFs. After several thousand iterations spanning the entire parameter space of physical and biogeochemical characteristics, a database of hypothetical worldwide N dynamics, including N_2O production and emissions, is generated for river, lake, reservoir, and estuarine systems. Then, global relationships relating N processes and N_2O emissions to TN and TP loads and water residence time are fitted from the database and applied for the global upscaling.

To calculate the cascading loads of TN and TP delivered to each water body along the river–reservoir–estuary continuum, we spatially routed all reservoirs from the GRanD database[77], with river networks from Hydrosheds 15s[78] and, at latitudes above 50°N, Hydro1K (USGS, 2000), which were in turn connected to estuaries as represented in the "Worldwide Typology of Nearshore Coastal Systems" of Dürr et al.[79]. In addition, the global data base HydroLAKES[76] was used to topologically connect 1.4 million lakes with a minimum surface area of 0.1 km^2 within the river network. Note that besides natural lakes, HydroLAKES includes updated information on 6,796 reservoirs from the GRanD data base, which was used in the study of Maavara et al.[10]. In order to estimate the TN and TP loads to each water body, we then relied on a spatially explicit representation of TN and TP mobilization from the watershed into the river network (see Maavara et al. for details[80,81]).

For the estimation of N_2O emission, we applied two distinct model configurations, respectively named DS1 and DS2 in Maavara et al.[10]. DS1 estimates N_2O emissions from denitrification and nitrification based on an EF of 0.9%, which is in the mean of published values[82], and the assumption that N_2O production equals N_2O emissions[10]. For DS2, the reduction of N_2O to N_2 during denitrification if N_2O is not evading sufficiently rapidly from the water body is taken into account. The fluxes in the model represent lumped sediment-water column rates and were resolved at the annual timescale. The use of water residence time as independent variable in both the mechanistic model and the upscaling process introduces an important kinetic refinement to existing global N_2O emission estimates. Rather than applying an average EF (directly scaling N_2O emissions to N inputs) to all water bodies, the use of water

residence time explicitly adjusts for the extent of N_2O production and emission that is kinetically possible within the timeframe available in a given water body. Simulated N_2O emission rates were evaluated against measurement-based upscaling methods applied to reservoirs[83] and rivers[84] as well as against observation-driven regional estimates of lake N_2O emissions based on literature data[9].

d. Coastal zone emissions

The average of net N_2O fluxes from three seagrass species[27] (seagrasses, mangroves, saltmarsh and intertidal) was scaled to the global seagrass area[28]. The mangrove data from Murray et al.[28] was updated with water-air and sediment-air N_2O fluxes from Maher et al.[85] and Murray et al.[86]. The average sediment-air N_2O flux and the average water-air N_2O flux were each applied for 12 hours a day (see Rosentreter et al.[87]), and scaled to the global mangrove area[28]. Murray et al.[28] saltmarsh data was updated with sediment-air N_2O fluxes from Yang et al.[88], Chmura et al.[89], Welti et al.[90] and Roughan et al.[91] and scaled to the global saltmarsh area[28]. Murray et al.[28] intertidal data was updated with sediment-air N_2O fluxes from Moseman-Valtierra et al. [92] and Sun et al.[93] and scaled to the global intertidal area[94].

2.10. Atmospheric inversion models

Emissions were estimated using four independent atmospheric inversion frameworks (see Supplementary Table 19). The frameworks all used the Bayesian inversion method, which finds the optimal emissions, that is, those, which when coupled to a model of atmospheric transport, provide the best agreement to observed N_2O mixing ratios while being guided by the prior estimates and their uncertainty. In other words, the optimal emissions are those that minimize the cost function:

$$J(\mathbf{x}) = \frac{1}{2}\left(\mathbf{x}-\mathbf{x_b}\right)^{\mathrm{T}}\mathbf{B}^{-1}\left(\mathbf{x}-\mathbf{x_b}\right) + \frac{1}{2}\left(\mathbf{y}-H(\mathbf{x})\right)^{\mathrm{T}}\mathbf{R}^{-1}\left(\mathbf{y}-H(\mathbf{x})\right) \quad (5a)$$

where $\mathbf{x}$ and $\mathbf{x_b}$ are, respectively, vectors of the optimal and prior emissions, $\mathbf{B}$ is the prior error covariance matrix, $\mathbf{y}$ is a vector of observed N_2O mixing ratios, $\mathbf{R}$ is the observation error covariance matrix, and $H(\mathbf{x})$ is the model of atmospheric transport (for details on the inversion

method see[95]). The optimal emissions, **x**, were found by solving the first order derivative of equation (5a):

$$J'(\mathbf{x}) = \mathbf{B}^{-1}\left(\mathbf{x} - \mathbf{x_b}\right) + \left(H'(\mathbf{x})\right)^{\mathrm{T}} \mathbf{R}^{-1}\left(\mathbf{y} - H(\mathbf{x})\right) = 0 \qquad (5b)$$

where $(H'(\mathbf{x}))^{\mathrm{T}}$ is the adjoint model of transport. In frameworks INVICAT, PyVAR and GEOSChem, equation (5b) was solved using the variational approach[96-98], which uses a descent algorithm and computations involving the forward and adjoint models. In framework MIROC4-ACTM, equation (5b) was solved directly by computing a transport operator, **H** from integrations of the forward model, such that **Hx** is equivalent to $H(\mathbf{x})$, and taking the transpose of **H**[99].

Each of the inversion frameworks used a different model of atmospheric transport with different horizontal and vertical resolutions (see Supplementary Table 19). The transport models TOMCAT and LMDz5, used in INVICAT and PyVAR respectively, were driven by ECMWF ERA-Interim wind fields, MIROC4-ACTM, was driven by JRA-55 wind fields, and GEOSChem was driven by MERRA-2 wind fields. While INVICAT, PyVAR, and GEOSChem optimized the emissions at the spatial resolution of the transport model, MIROC4-ACTM optimized the error in the emissions aggregated into 84 land and ocean regions. All frameworks optimized the emissions with monthly temporal resolution. The transport models included an online calculation of the loss of N_2O in the stratosphere due to photolysis and oxidation by $O(^1D)$ resulting in mean atmospheric lifetimes of between 118 and 129 years, broadly consistent with recent independent estimates of the lifetime of 116±9 years (ref. [100]).

All inversions used N_2O measurements of discrete air samples from the National Oceanic and Atmospheric Administration Carbon Cycle Cooperative Global Air Sampling Network (NOAA). In addition, discrete measurements from the Commonwealth Scientific and Industrial Research Organisation network (CSIRO) as well as in-situ measurements from the Advanced Global Atmospheric Gases Experiment network (AGAGE), the NOAA CATS network, and from individual sites operated by University of Edinburgh (UE), National Institute for Environmental Studies (NIES) and the Finnish Meteorological Institute (FMI) were included in INVICAT, PyVAR and GEOSchem. Measurements from networks other than NOAA were corrected to the NOAA calibration scale, NOAA-2006A, using the results of the WMO Round Robin inter-

comparison experiment (https://www.esrl.noaa.gov/gmd/ccgg/wmorr/), where available. For AGAGE and CSIRO, which did not participate in the WMO Round Robins, the data at sites where NOAA discrete samples are also collected were used to calculate a linear regression with NOAA data, which was applied to adjust the data to the NOAA-2006A scale. For the remaining CSIRO sites where there were no NOAA discrete samples, the mean regression coefficient and offset from all other CSIRO sites were used. The inversions used the discrete sample measurements without averaging, and hourly or daily means of the in-situ measurements, depending on the particular inversion framework.

Each framework applied its own method for calculating the observation space uncertainty, the square of which gives the diagonal elements of the observation error covariance matrix **R**. The observation space uncertainty accounts for measurement and model representation errors and is equal to the quadratic sum of these terms. Typical values for the observation space uncertainty were between 0.3 and 0.5 ppb for all inversion frameworks.

Prior emissions were based on estimates from terrestrial biosphere and ocean biogeochemistry models as well as from inventories. INVICAT, PyVAR and GEOSChem used the same prior estimates for emissions from natural and agricultural soils from the model OCN v1.1[22] and for biomass burning emissions from GFEDv4.1s. For non-soil anthropogenic emissions (namely those from energy, industry and waste sectors), INVICAT and GEOSChem used EDGAR v4.2FT2010 and PyVAR used EDGAR v4.3.2. MIROC4-ACTM used the VISIT model[24,25] for emissions from natural soils and EDGAR 4.2 for all anthropogenic emissions, including agricultural burning, but did not explicitly include a prior estimate for wildfire emissions.

Three different prior estimates for ocean emissions were used: 1) from the ocean biogeochemistry model, NEMO-PlankTOM5[101], with a global total of 6.6 Tg N yr^{-1}, 2) from the updated version of this model, NEMO-PlankTOM10[5] with a global total of 3.7 Tg N yr^{-1}, and 3) from the MIT ocean general circulation model, as described by Manizza et al.[102] with a global total of 3.8 Tg N yr^{-1}.

Prior uncertainties were estimated in all the inversion frameworks for each grid cell (INVICAT, PyVAR and GEOSChem) or for each region (MIROC4-ACTM) and square of the uncertainties formed the diagonal elements of the prior error covariance matrix **B**. INVICAT, PyVAR and GEOSChem estimated the uncertainty as proportional to the prior value in each grid

cell, but MIROC4-ACTM set the uncertainty uniformly for the land regions at 1 Tg N yr^{-1} and for the ocean regions at 0.5 Tg N yr^{-1}.

3. Atmospheric N_2O observations and growth rates for three different atmospheric networks (NOAA, AGAGE, and CISRO)

The monthly atmospheric N_2O abundances and their growth rates are derived from three different atmospheric observational networks (AGAGE, CISRO and NOAA) (Extended Data Fig. 1).

For atmospheric N_2O observations from the NOAA network[103], we used global mean mixing ratios from the GMD combined dataset during 1980–2017 based on measurements from five different measurement programs [HATS old flask instrument, HATS current flask instrument (OTTO), CCGG group Cooperative Global Air Sampling Network (https://www.esrl.noaa.gov/gmd/ccgg/flask.php), HATS *in situ* (RITS program), and HATS *in situ* (CATS program)]. CCGG provides uncertainties with each measurement (see site files: ftp://aftp.cmdl.noaa.gov/data/greenhouse_gases/n2o/flask/surface/). Global means are derived from flask and *in situ* measurements obtained by gas chromatography with electron capture detection, from 4–12 sites (fewer sites in the earlier years), weighted by representative area. Monthly mean observations from different NOAA measurement programs are statistically combined to create a long-term NOAA/ESRL GMD dataset. Uncertainties (1 sigma) associated with monthly estimates of global mean N_2O, are ~1 ppb from 1977–1987, 0.6 ppb from 1988–1994, 0.3–0.4 ppb from 1995–2000, and 0.1 ppb from 2001–2017. NOAA data are generally more consistent after 1995, with standard deviations on the monthly mean mixing ratios at individual sites of ~0.5 ppb from 1995–1998, and 0.1–0.4 ppb after 1998. A detailed description of these measurement programs and the method to combine them are available via https://www.esrl.noaa.gov/gmd/hats/combined/N2O.html.

The Advanced Global Atmospheric Gases Experiment (AGAGE) global network (and its predecessors ALE and GAGE)[104] has made continuous high frequency gas chromatographic measurements of N_2O at five globally distributed sites since 1978. AGAGE includes two types of instruments [i.e., a gas chromatograph with multiple detectors (GC-MD) and a gas

chromatograph with preconcentration and mass spectrometric analysis (Medusa GC-MS)]. The measurement precision for N_2O improved from about 0.35% in ALE to 0.13% in GAGE[105] and 0.05% in AGAGE[104]. We used the global mean of N_2O measurements from the GC-MD during 1980–2017. Further information on AGAGE stations, instruments, calibration, uncertainties and access to data is available at the AGAGE website: http://agage.mit.edu.

The CSIRO flask network[106] consists of nine sampling sites distributed globally and has been in operation since 1992. Flask samples are collected approximately every two weeks and shipped back to CSIRO GASLAB for analysis. Samples were analyzed by gas chromatography with electron capture detection (GC-ECD). One Shimadzu gas chromatograph, labelled "Shimadzu-1" (S1) was used over the entire length of the record and the measurement precision for N_2O from this instrument is about 0.1%. N_2O data from the CSIRO global flask network are reported on the NOAA-2006A N_2O scale and are archived at the World Data Centre for Greenhouse Gases (WDCGG: https://gaw.kishou.go.jp/). Nine sites from the CSIRO network were used to calculate the annual global N_2O mole fractions. Smooth curve fits to the N_2O data from each of these sites were calculated using the technique outlined in Thoning et al.[107], using a short-term cut-off of 80 days. The smooth curve fit data were then placed on an evenly spaced latitude (5 degree) versus time (weekly) grid using the Kriging interpolation technique. Finally, the gridded data were used to calculate the global annual average mole fractions weighted by latitude.

We plotted the atmospheric globally averaged N_2O abundances and the associated growth rates for the three global atmospheric networks NOAA, AGAGE, and CSIRO during 1980–2017 (see Extended Data Fig. 1). We see remarkably consistent global mean N_2O estimated from the three different networks, increasing from 301.0±0.1 ppb in 1980 to 329.9±0.4 ppb in 2017. Growth rates of N_2O are also remarkably consistent among the three measurement networks. After a period in the late 1990s in which the growth rate averaged about 0.8 ppb yr^{-1}, the global growth rate fell to ~0.6 ppb yr^{-1} and then gradually increased to nearly 1 ppb yr^{-1} by 2013–2017. Interannual variability in the N_2O growth rate was higher prior to 1995 (not shown) than after 1995, which may be an artifact of less precise measurements due to changes in instrumental precision and measurement frequency over the study period. Additional discussion on uncertainties associated with measurement errors and emission errors in inversions can be found in Chen and Prinn[108] and Thompson et al[16].

4. Comparison with the IPCC AR5

Our methodology significantly differs from past approaches summarized in the IPCC AR5. Most of the estimates used in the AR5 (e.g., natural sources) directly inherited or adopted with minor revisions data from studies conducted mainly in the 1990s. Some estimates used in the IPCC AR5 (e.g., atmospheric deposition on land) were from a review by Syakila and Kroeze[109], which depended on empirical methods and simple assumptions.

Compared to the findings reported in the IPCC AR5, our budget includes several new sources (e.g., aquaculture, deforestation/post-deforestation, the effects of environmental factors, natural sources of inland and coastal waters) and one additional (tropospheric) sink for N_2O (Table 6). We report natural sources of N_2O emissions from inland and coastal waters with a value of 0.3 Tg N yr^{-1}. The total source of N_2O in our study is 0.9 Tg N yr^{-1} smaller than that in the IPCC AR5, while our estimate of anthropogenic N_2O emissions is 0.4 Tg N yr^{-1} larger in the recent decade (Supplementary Table 15). Our larger estimate of anthropogenic emissions is associated with environmental effects (0.2, with a range of -0.6 to 1.1 Tg N yr^{-1}, based on NMIP simulations), and a 0.4 Tg N yr^{-1} larger estimate of atmospheric N deposition emissions (based on modeling results and inventories, Table 1). In contrast, our estimate of direct emissions from agriculture [(3.8 (2.5–5.8) Tg N yr^{-1}, plus aquaculture, a minor contribution] is 0.3 Tg N yr^{-1} smaller than reported in the IPCC AR5.

Natural sources in our study are 1.3 Tg N yr^{-1} smaller than those reported by the IPCC AR5 for 2007–2016 and the range is significantly reduced. The mean NMIP estimate of global natural soil emission [5.6 (4.9–6.6) Tg N yr^{-1}] is 1.0 Tg N yr^{-1} smaller compared to those in the IPCC AR5 estimate [6.6 (3.3–9.0) Tg N yr^{-1}]. The reduction in uncertainty in NMIP estimates may result from calibration of terrestrial biosphere models in NMIP against in situ observations across the globe[1], while the AR5 estimate, essentially inherited from the AR4 synthesis, was based on results from a single simple model by Bouwman et al.[110].

In this study, global oceanic N_2O emission is derived from an ensemble of global ocean biogeochemistry models. Our estimate [3.4 (2.5–4.3) Tg N yr^{-1}] is 0.4 Tg N yr^{-1} smaller and the uncertainty range is significantly smaller than reported in the IPCC AR5 (1.8–9.4 Tg N yr^{-1}). The larger AR5 range was determined using an analysis of Atlantic Ocean surface measurements (Rhee et al.[111]; the Atlantic is not a region of significant N_2O emission) as the lower bound, and the upper bound was the maximal value of N_2O production from a global empirically based analysis[112]. The parameterizations governing marine productivity and N_2O yield in our five ocean models have been constrained by a variety of datasets characterizing marine biogeochemical process rates, and the model simulations of ocean N_2O have been evaluated against global biogeochemical databases (e.g., see Battaglia and Joos[3] and Buitenhuis et al.[5] for more detail). The smaller range of ocean N_2O emission reported in this study includes advances in modeling such factors as quantification of global marine export production, improved constraints on N_2O yield parameters (particularly in the well-oxygenated ocean), and more comprehensive evaluation of modeled biogeochemical distributions.

The estimated N_2O production through atmospheric chemistry is 0.2 Tg N yr^{-1} smaller than reported in the IPCC AR5. The observed stratospheric sink of N_2O in this study is 0.9 Tg N yr^{-1} smaller than in the IPCC AR5, wherein stratospheric N_2O destruction was tuned to be consistent with the difference between the total source and the observed atmospheric N_2O growth rate. In our study, stratospheric sinks were obtained from atmospheric chemistry transport models and the recent post-AR5 study by Prather et al.[16,100,113] who calculated N_2O stratospheric loss (& lifetime) based on satellite observations combined with simple photolysis models using observed atmospheric temperature, O_2, and O_3. Our uncertainties in the atmospheric loss of N_2O (±1.1 Tg N yr^{-1}) are slightly larger than those of the AR5 (±0.9 Tg N yr^{-1}). In our study, annual change in atmospheric abundance is calculated from the combined NOAA and AGAGE record of surface N_2O and uncertainty (±0.5 Tg N yr^{-1}) is taken from the IPCC AR5 (ref. [114]).

5. Per capita N_2O emission at global and regional scales in the recent decade

Per capita N_2O emission is calculated using global and regional emissions divided by the numbers of global and regional population[115] (see Supplementary Fig. 2). Global per capita emissions from top-down and bottom-up approaches were on average ~2 kg N $capita^{-1}$ yr^{-1} in the

recent decade. Bottom-up estimates show that per capita natural fluxes including natural soils and inland and coastal waters were the largest source, followed by agriculture and other direct anthropogenic sources. South America and Oceania have ~2 times and ~6 times higher per capita emissions than the global average, respectively. Africa and Russia also have higher per capita N_2O emissions than the global value contributed primarily by natural fluxes and to a minor extent by other direct anthropogenic sources (Africa: Biomass burning; Russia: Fossil fuel and industry and Biomass burning). In addition, North America and Europe show higher than global per capita emissions from agriculture and other direct anthropogenic sources (primary from Fossil fuel and industry). Middle East, East Asia, South Asia, and Southeast Asia show lower than global per capita emissions from all sources.

References:

1 Tian, H. Q. *et al.* Global soil nitrous oxide emissions since the preindustrial era estimated by an ensemble of terrestrial biosphere models: Magnitude, attribution, and uncertainty. *Global Change Biology* **25**, 640-659 (2019).

2 Dangal, S. R. *et al.* Global nitrous oxide emissions from pasturelands and rangelands: Magnitude, spatio-temporal patterns and attribution. *Global Biogeochemical Cycles* **33**, 200-222 (2019).

3 Battaglia, G. & Joos, F. Marine N_2O Emissions From Nitrification and Denitrification Constrained by Modern Observations and Projected in Multimillennial Global Warming Simulations. *Global Biogeochemical Cycles* **32**, 92-121 (2018).

4 Berthet, S. *et al.* Evaluation of an Online Grid-Coarsening Algorithm in a Global Eddy-Admitting Ocean Biogeochemical Model. *Journal of Advances in Modeling Earth Systems* **11**, 1759-1783 (2019).

5 Buitenhuis, E. T., Suntharalingam, P. & Le Quéré, C. Constraints on global oceanic emissions of N_2O from observations and models. *Biogeosciences* **15**, 2161-2175 (2018).

6 Landolfi, A., Somes, C. J., Koeve, W., Zamora, L. M. & Oschlies, A. Oceanic nitrogen cycling and N_2O flux perturbations in the Anthropocene. *Global Biogeochemical Cycles* **31**, 1236-1255 (2017).

7 Martinez-Rey, J., Bopp, L., Gehlen, M., Tagliabue, A. & Gruber, N. Projections of oceanic N_2O emissions in the 21st century using the IPSL Earth system model. *Biogeosciences* **12**, 4133-4148 (2015).

8 Suntharalingam, P. *et al.* Estimates of Oceanic Nitrous-oxide Emissions from Global Biogeochemistry Models. *American Geophysical Union, Fall Meeting 2018* (2018).

9 Lauerwald, R. *et al.* Natural lakes are a minor global source of N_2O to the atmosphere. *Global Biogeochemical Cycles* **33**, 1564-1581 (2019).

10 Maavara, T. *et al.* Nitrous oxide emissions from inland waters: Are IPCC estimates too high? *Global Change Biology* **25**, 473-488 (2019).

11 Janssens-Maenhout, G. *et al.* EDGAR v4.3.2 Global Atlas of the three major greenhouse gas emissions for the period 1970–2012. *Earth System Science Data* **11**, 959-1002 (2019).

12 Tubiello, F. *et al.* Estimating greenhouse gas emissions in agriculture: a manual to address data requirements for developing countries. FAO, Rome (2015).

13 Winiwarter, W., Höglund-Isaksson, L., Klimont, Z., Schöpp, W. & Amann, M. Technical opportunities to reduce global anthropogenic emissions of nitrous oxide. *Environmental research letters* **13**, 014011 (2018).

14 Van Der Werf, G. R. *et al.* Global fire emissions estimates during 1997-2016. *Earth System Science Data* **9**, 697-720 (2017).

15 Wang, Q. *et al.* Data-driven estimates of global nitrous oxide emissions from croplands. *National Science Review* **00**, 1-12 (2019).

16 Thompson, R. L. *et al.* Acceleration of global N_2O emissions seen from two decades of atmospheric inversion. *Natural Climate Change* **9**, 993-998 (2019).

17 Tian, H. Q. *et al.* The Global N_2O Model Intercomparison Project. *Bulletin of the American Meteorological Society* **99**, 1231-1252 (2018).

18 Tian, H. *et al.* Global methane and nitrous oxide emissions from terrestrial ecosystems due to multiple environmental changes. *Ecosystem Health and Sustainability* **1**, 1-20 (2015).

19 Xu, R. *et al.* Preindustrial nitrous oxide emissions from the land biosphere estimated by using a global biogeochemistry model. *Climate of the Past* **13**, 977 (2017).

20 Stocker, B. D. *et al.* Multiple greenhouse-gas feedbacks from the land biosphere under future climate change scenarios. *Nature Climate Change* **3**, 666, doi:10.1038/nclimate1864 (2013).

21 XU-RI & PRENTICE, I. C. Terrestrial nitrogen cycle simulation with a dynamic global vegetation model. *Global Change Biology* **14**, 1745-1764 (2008).

22 Zaehle, S., Ciais, P., Friend, A. D. & Prieur, V. Carbon benefits of anthropogenic reactive nitrogen offset by nitrous oxide emissions. *Nature Geoscience* **4**, 601-605 (2011).
23 Goll, D. S. *et al.* A representation of the phosphorus cycle for ORCHIDEE (revision 4520). *Geosci. Model Dev.* **10**, 3745-3770 (2017).
24 Inatomi, M., Ito, A., Ishijima, K. & Murayama, S. Greenhouse Gas Budget of a Cool-Temperate Deciduous Broad-Leaved Forest in Japan Estimated Using a Process-Based Model. *Ecosystems* **13**, 472-483 (2010).
25 Ito, A., Nishina, K., Ishijima, K., Hashimoto, S. & Inatomi, M. Emissions of nitrous oxide (N_2O) from soil surfaces and their historical changes in East Asia: a model-based assessment. *Progress in Earth and Planetary Science* **5**, 55, doi:10.1186/s40645-018-0215-4 (2018).
26 Yao, Y. *et al.* Increased global nitrous oxide emissions from streams and rivers in the Anthropocene. *Natural Climate Change* **10**, 138-142 (2020).
27 Camillini, N., Rossentreter, J., Erler, D., Glud, R. N. & Eyre, B. Blue carbon burial in seagrass meadows is partially offset by CH_4 and N_2O fluxes. *Science Advance* (Submitted).
28 Murray, R. H., Erler, D. V. & Eyre, B. D. Nitrous oxide fluxes in estuarine environments: response to global change. *Global Change Biology* **21**, 3219-3245 (2015).
29 Beusen, A. H., Bouwman, A. F., Van Beek, L. P., Mogollón, J. M. & Middelburg, J. J. Global riverine N and P transport to ocean increased during the 20th century despite increased retention along the aquatic continuum. *Biogeosciences* **13**, 2441-2451 (2016).
30 Bouwman, A. F. *et al.* Hindcasts and future projections of global inland and coastal nitrogen and phosphorus loads due to finfish aquaculture. *Reviews in Fisheries Science* **21**, 112-156 (2013).
31 Bouwman, A. F. *et al.* Global hindcasts and future projections of coastal nitrogen and phosphorus loads due to shellfish and seaweed aquaculture. *Reviews in Fisheries Science* **19**, 331-357 (2011).
32 Tubiello, F. N. *et al.* The FAOSTAT database of greenhouse gas emissions from agriculture. **8**, 015009 (2013).
33 Davidson, E. A., Erickson, H. E., Verchot, L. V., Keller, M. & Veldkamp, E. Testing a Conceptual Model of Soil Emissions of Nitrous and Nitric Oxides: Using two functions based on soil nitrogen availability and soil water content, the hole-in-the-pipe model characterizes a large fraction of the observed variation of nitric oxide and nitrous oxide emissions from soils. *BioScience* **50**, 667-680 (2000).
34 IPCC. 2006 IPCC Guidelines for National Greenhouse Gas Inventories., (Japan on behalf of the IPCC, Hayama, Japan, 2006).
35 Zhou, J., Jiang, M. & Chen, G. Estimation of methane and nitrous oxide emission from livestock and poultry in China during 1949–2003. *Energy Policy* **35**, 3759-3767 (2007).
36 Van Drecht, G., Bouwman, A. F., Knoop, J. M., Beusen, A. H. W. & Meinardi, C. R. Global modeling of the fate of nitrogen from point and nonpoint sources in soils, groundwater, and surface water. *Global Biogeochemical Cycles* **17**, 1115, doi:10.1029/2003gb002060 (2003).
37 Amann, M. *et al.* Cost-effective control of air quality and greenhouse gases in Europe: Modeling and policy applications. *Environmental Modelling & Software* **26**, 1489-1501 (2011).
38 Zhang, X. *et al.* Managing nitrogen for sustainable development. *Nature* **528**, 51, doi:doi:10.1038/nature15743 (2015).
39 Gao, S. *et al.* Quantifying nitrogen leaching response to fertilizer additions in China's cropland. *Environmental pollution* **211**, 241-251 (2016).
40 Hou, X. *et al.* Detection and attribution of nitrogen runoff trend in China's croplands. *Environmental pollution* **234**, 270-278 (2018).
41 Zhou, F. *et al.* New model for capturing the variations of fertilizer-induced emission factors of N2O. *Global Biogeochemical Cycles* **29**, 885-897 (2015).
42 Decock, C. Mitigating nitrous oxide emissions from corn cropping systems in the midwestern US: potential and data gaps. *Environmental science & technology* **48**, 4247-4256 (2014).

43 Harris, I., Jones, P. D., Osborn, T. J. & Lister, D. H. Updated high-resolution grids of monthly climatic observations–the CRU TS3. 10 Dataset. *International journal of climatology* **34**, 623-642 (2014).
44 Helgason, B. *et al.* Toward improved coefficients for predicting direct N_2O emissions from soil in Canadian agroecosystems. *Nutrient Cycling in Agroecosystems* **72**, 87-99 (2005).
45 Hénault, C. *et al.* Predicting in situ soil N_2O emission using NOE algorithm and soil database. *Global Change Biology* **11**, 115-127 (2005).
46 Hickman, J. E., Scholes, R. J., Rosenstock, T. S., Garcia-Pando, C. P. & Nyamangara, J. Assessing non-CO_2 climate-forcing emissions and mitigation in sub-Saharan Africa. *Current Opinion in Environmental Sustainability* **9**, 65-72 (2014).
47 Kim, D.-G., Giltrap, D. & Hernandez-Ramirez, G. Background nitrous oxide emissions in agricultural and natural lands: a meta-analysis. *Plant and soil* **373**, 17-30 (2013).
48 Kim, D.-G., Hernandez-Ramirez, G. & Giltrap, D. Linear and nonlinear dependency of direct nitrous oxide emissions on fertilizer nitrogen input: A meta-analysis. *Agriculture, Ecosystems & Environment* **168**, 53-65 (2013).
49 Lehuger, S. *et al.* Predicting and mitigating the net greenhouse gas emissions of crop rotations in Western Europe. *Agricultural and forest meteorology* **151**, 1654-1671 (2011).
50 Leppelt, T. *et al.* Nitrous oxide emission budgets and land-use-driven hotspots for organic soils in Europe. *Biogeosciences* (2014).
51 Rochette, P. & Janzen, H. H. Towards a revised coefficient for estimating N_2O emissions from legumes. *Nutrient Cycling in Agroecosystems* **73**, 171-179 (2005).
52 Sacks, W. J., Deryng, D., Foley, J. A. & Ramankutty, N. Crop planting dates: an analysis of global patterns. *Global Ecol Biogeogr* **19**, 607-620 (2010).
53 Shcherbak, I., Millar, N. & Robertson, G. P. Global metaanalysis of the nonlinear response of soil nitrous oxide (N_2O) emissions to fertilizer nitrogen. *Proceedings of the National Academy of Sciences* **111**, 9199-9204 (2014).
54 Stehfest, E. & Bouwman, L. N_2O and NO emission from agricultural fields and soils under natural vegetation: summarizing available measurement data and modeling of global annual emissions. *Nutrient Cycling in Agroecosystems* **74**, 207-228 (2006).
55 Walter, K. *et al.* Direct nitrous oxide emissions from oilseed rape cropping–a meta-analysis. *GCB Bioenergy* **7**, 1260-1271 (2015).
56 Berdanier, A. B. & Conant, R. T. Regionally differentiated estimates of cropland N_2O emissions reduce uncertainty in global calculations. *Global change biology* **18**, 928-935 (2012).
57 Yang, H. *et al.* Regional patterns of future runoff changes from Earth system models constrained by observation. *Geophysical Research Letters* **44**, 5540-5549 (2017).
58 Goldewijk, K. K., Beusen, A., Doelman, J. & Stehfest, E. Anthropogenic land use estimates for the Holocene–HYDE 3.2. *Earth System Science Data* **9**, 927-953 (2017).
59 Zhang, B. *et al.* Global manure nitrogen production and application in cropland during 1860–2014: a 5 arcmin gridded global dataset for Earth system modeling. *Earth System Science Data* **9,** 667-678 (2017).
60 Rosas, F. Fertilizer use by crop at the country level (1990–2010). *CARD Working Papers* **555** (2012).
61 Carlson, K. M. *et al.* Greenhouse gas emissions intensity of global croplands. *Nature Climate Change* **7**, 63 (2017).
62 Bouwman, L. *et al.* Mariculture: significant and expanding cause of coastal nutrient enrichment. *Environmental Research Letters* **8**, 044026, doi:044010.041088/041748-049326/044028/044024/044026 (2013).
63 Bouwman, A. F. *et al.* Hindcasts and future projections of global inland and coastal nitrogen and phosphorus loads due to finfish aquaculture. *Reviews in Fisheries Science* **21**, 112-156 (2013).
64 Bouwman, A. F. *et al.* Global hindcasts and future projections of coastal nitrogen and phosphorus loads due to shellfish and seaweed aquaculture. *Reviews in Fisheries Science* **19**, 331-357 (2011).

65 FAO. FishStatJ - Software for Fishery and Aquaculture Statistical Time Series. http://www.fao.org/fishery/statistics/software/fishstatj/en. (Fisheries and Aquaculture Information and Statistics Service, Food and Agriculture Organization of the United Nations, retrieved 22 May 2019, Rome, 2019).
66 Sullivan, B. W. *et al.* Biogeochemical recuperation of lowland tropical forest during succession. *Ecology* **100**, e02641, doi:10.1002/ecy.2641 (2019).
67 Davidson, E. A. *et al.* Recuperation of nitrogen cycling in Amazonian forests following agricultural abandonment. *Nature* **447**, 995 (2007).
68 Keller, M. & Reiners, W. A. Soil-atmosphere exchange of nitrous oxide, nitric oxide, and methane under secondary succession of pasture to forest in the Atlantic lowlands of Costa Rica. *Global Biogeochemical Cycles* **8**, 399-409 (1994).
69 Liu, M. *et al.* Long-term trends in evapotranspiration and runoff over the drainage basins of the Gulf of Mexico during 1901–2008. *Water Resources Research* **49**, 1988-2012 (2013).
70 Ren, W. *et al.* Century-long increasing trend and variability of dissolved organic carbon export from the Mississippi River basin driven by natural and anthropogenic forcing. *Global Biogeochemical Cycles* **30**, 1288-1299 (2016).
71 Ren, W. *et al.* Large increase in dissolved inorganic carbon flux from the Mississippi River to Gulf of Mexico due to climatic and anthropogenic changes over the 21st century. *Journal of Geophysical Research: Biogeosciences* **120**, 724-736 (2015).
72 Tao, B. *et al.* Increasing Mississippi river discharge throughout the 21st century influenced by changes in climate, land use, and atmospheric CO_2. *Geophysical Research Letters* **41**, 4978-4986 (2014).
73 Tian, H. *et al.* Climate extremes dominating seasonal and interannual variations in carbon export from the Mississippi River Basin. *Global Biogeochemical Cycles* **29**, 1333-1347 (2015).
74 Tian, H. *et al.* Anthropogenic and climatic influences on carbon fluxes from eastern North America to the Atlantic Ocean: A process-based modeling study. *Journal of Geophysical Research: Biogeosciences* **120**, 757-772 (2015).
75 Yang, Q. *et al.* Increased nitrogen export from eastern North America to the Atlantic Ocean due to climatic and anthropogenic changes during 1901–2008. *Journal of Geophysical Research: Biogeosciences* **120**, 1046-1068 (2015).
76 Messager, M. L., Lehner, B., Grill, G., Nedeva, I. & Schmitt, O. Estimating the volume and age of water stored in global lakes using a geo-statistical approach. *Nature Communications* **7**, 13603 (2016).
77 Lehner, B. *et al.* High-resolution mapping of the world's reservoirs and dams for sustainable river-flow management. *Frontiers in Ecology and the Environment* **9**, 494-502 (2011).
78 Lehner, B., Verdin, K. & Jarvis, A. New global hydrography derived from spaceborne elevation data. *Eos, Transactions, American Geophysical Union* **89**, 93-94 (2008).
79 Dürr, H. H. *et al.* Worldwide Typology of Nearshore Coastal Systems: Defining the Estuarine Filter of River Inputs to the Oceans. *Estuaries and Coasts* **34**, 441-458 (2011).
80 Bouwman, A., Beusen, A. H. & Billen, G. J. G. B. C. Human alteration of the global nitrogen and phosphorus soil balances for the period 1970–2050. *Global Biogeochemical Cycles* **23,** GB0A04, doi:10.1029/2009GB003576 (2009).
81 Van Drecht, G., Bouwman, A., Harrison, J. & Knoop, J. Global nitrogen and phosphate in urban wastewater for the period 1970 to 2050. *Global Biogeochemical Cycles* **23**, GB0A03 (2009).
82 Beaulieu, J. J. *et al.* Nitrous oxide emission from denitrification in stream and river networks. *Proceedings of the National Academy of Sciences* **108**, 214-219 (2011).
83 Deemer, B. R. *et al.* Greenhouse gas emissions from reservoir water surfaces: a new global synthesis. **66**, 949-964 (2016).
84 Hu, M., Chen, D. & Dahlgren, R. A. Modeling nitrous oxide (N_2O) emission from rivers: A global assessment. *Global Change Biology* **22**, 3566-3582 (2016).

85 Maher, D. T., Sippo, J. Z., Tait, D. R., Holloway, C. & Santos, I. R. Pristine mangrove creek waters are a sink of nitrous oxide. *Scientific reports* **6**, 25701 (2016).
86 Murray, R., Erler, D., Rosentreter, J., Maher, D. & Eyre, B. A seasonal source and sink of nitrous oxide in mangroves: Insights from concentration, isotope, and isotopomer measurements. *Geochimica et Cosmochimica Acta* **238**, 169-192 (2018).
87 Rosentreter, J. A., Maher, D. T., Erler, D. V., Murray, R. H. & Eyre, B. D. Methane emissions partially offset "blue carbon" burial in mangroves. *Science advances* **4**, eaao4985 (2018).
88 Yang, W. H. & Silver, W. L. Gross nitrous oxide production drives net nitrous oxide fluxes across a salt marsh landscape. *Global Change Biology* **22**, 2228-2237 (2016).
89 Chmura, G. L., Kellman, L., Van Ardenne, L. & Guntenspergen, G. R. Greenhouse gas fluxes from salt marshes exposed to chronic nutrient enrichment. *PloS one* **11**, e0149937 (2016).
90 Welti, N., Hayes, M. & Lockington, D. Seasonal nitrous oxide and methane emissions across a subtropical estuarine salinity gradient. *Biogeochemistry* **132**, 55-69 (2017).
91 Roughan, B. L., Kellman, L., Smith, E. & Chmura, G. L. Nitrous oxide emissions could reduce the blue carbon value of marshes on eutrophic estuaries. *Environmental Research Letters* **13**, 044034 (2018).
92 Moseman-Valtierra, S. *et al.* Substantial nitrous oxide emissions from intertidal sediments and groundwater in anthropogenically-impacted West Falmouth Harbor, Massachusetts. *Chemosphere* **119**, 1281-1288 (2015).
93 Sun, W., Sun, Z., Mou, X., Sun, W. & Hu, X. Nitrous oxide emissions from intertidal zone of the Yellow River estuary in autumn and winter during 2011–2012. *Estuaries and coasts* **40**, 145-159 (2017).
94 Murray, N. J. *et al.* The global distribution and trajectory of tidal flats. *Nature* **565**, 222 (2019).
95 Tarantola, A. *Inverse problem theory and methods for model parameter estimation*. Vol. 89 (Society for Industrial and Applied Mathematics 2005).
96 Thompson, R. L. *et al.* Nitrous oxide emissions 1999 to 2009 from a global atmospheric inversion. *Atmospheric Chemistry and Physics* **14**, 1801-1817 (2014).
97 Wells, K. C. *et al.* Simulation of atmospheric N_2O with GEOS-Chem and its adjoint: evaluation of observational constraints. *Geoscience Model Development* **8**, 3179-3198 (2015).
98 Wilson, C., Chipperfield, M., Gloor, M. & Chevallier, F. Development of a variational flux inversion system (INVICAT v1. 0) using the TOMCAT chemical transport model. *Geoscientific Model Development* **7**, 2485-2500 (2014).
99 Patra, P. K. *et al.* Improved Chemical Tracer Simulation by MIROC4. 0-based Atmospheric Chemistry-Transport Model (MIROC4-ACTM). *Sola* **14**, 91-96 (2018).
100 Prather, M. J. *et al.* Measuring and modeling the lifetime of nitrous oxide including its variability. *Journal of Geophysical Research: Atmospheres* **120**, 5693-5705 (2015).
101 Suntharalingam, P. *et al.* Quantifying the impact of anthropogenic nitrogen deposition on oceanic nitrous oxide. *Geophysical Research Letters* **39,** L07605, doi:10.1029/2011GL050778 (2012).
102 Manizza, M., Keeling, R. F. & Nevison, C. D. On the processes controlling the seasonal cycles of the air–sea fluxes of O_2 and N_2O: A modelling study. *Tellus B: Chemical and Physical Meteorology* **64**, 18429, doi:10.3402/tellusb.v64i0.18429 (2012).
103 Hall, B., Dutton, G. & Elkins, J. The NOAA nitrous oxide standard scale for atmospheric observations. *Journal of Geophysical Research: Atmospheres* **112**, D09305, doi:10.1029/2006JD007954 (2007).
104 Prinn, R. G. *et al.* History of chemically and radiatively important atmospheric gases from the Advanced Global Atmospheric Gases Experiment (AGAGE). *Earth System Science Data* **10**, 985-1018 (2018).
105 Prinn, R. *et al.* Atmospheric emissions and trends of nitrous oxide deduced from 10 years of ALE–GAGE data. *Journal of Geophysical Research: Atmospheres* **95**, 18369-18385 (1990).
106 Francey, R. J. *et al.* The CSIRO (Australia) measurement of greenhouse gases in the global atmosphere. 97-111 (World Meteorological Organization, Tokyo, Japan, 2003).

107 Thoning, K. W., Tans, P. P. & Komhyr, W. D. Atmospheric carbon dioxide at Mauna Loa Observatory: 2. Analysis of the NOAA GMCC data, 1974–1985. *Journal of Geophysical Research: Atmospheres* **94**, 8549-8565 (1989).
108 Chen, Y. H. & Prinn, R. G. Estimation of atmospheric methane emissions between 1996 and 2001 using a three-dimensional global chemical transport model. *Journal of Geophysical Research: Atmospheres* **111**, 307, doi:10.1029/2005JD006058 (2006).
109 Syakila, A. & Kroeze, C. The global nitrous oxide budget revisited. *Greenhouse Gas Measurement and Management* **1**, 17-26 (2011).
110 Bouwman, A., Fung, I., Matthews, E. & John, J. Global analysis of the potential for N_2O production in natural soils. *Global Biogeochemical Cycles* **7**, 557-597 (1993).
111 Rhee, T. S., Kettle, A. J. & Andreae, M. O. Methane and nitrous oxide emissions from the ocean: A reassessment using basin-wide observations in the Atlantic. *Journal of Geophysical Research: Atmospheres* **114**, doi:10.1029/2008jd011662 (2009).
112 Bianchi, D., Dunne, J. P., Sarmiento, J. L. & Galbraith, E. D. Data-based estimates of suboxia, denitrification, and N_2O production in the ocean and their sensitivities to dissolved O_2. *Global Biogeochemical Cycles* **26**, doi:10.1029/2011gb004209 (2012).
113 Prather, M. J. & Hsu, J. Coupling of Nitrous Oxide and Methane by Global Atmospheric Chemistry. *Science* **330**, 952-954 (2010).
114 Ciais, P. *et al.* in *Climate Change 2013: The Physical Science Basis. Contribution of Working Group I to the Fifth Assessment Report of the Intergovernmental Panel on Climate Change* 465-570 (Cambridge University Press, 2014).
115 FAOSTAT. *Food and Agriculture Organization of the United Nations Statistics-Population*, 2020).
116 Hu, Z., Lee, J. W., Chandran, K., Kim, S. & Khanal, S. K. Nitrous oxide (N_2O) emission from aquaculture: a review. *Environmental science technology* **46**, 6470-6480 (2012).
117 MacLeod, M., Hasan, M. R., Robb, D. H. F. & Mamun-Ur-Rashid, M. Quantifying and mitigating greenhouse gas emissions from global aquaculture. FAO, Rome, (2019).

Supplementary Table 1 N_2O emissions from global agricultural soils based on multiple bottom-up approaches including the additions of mineral N fertilizer, manure and crop residues, and cultivation of organic soils. Unit: Tg N yr^{-1}

Data sources		1980s	1990s	2000s	2007-2016
Process-based models	NMIP/DLEM Mean	1.7	2.1	2.4	2.8
	NMIP/DLEM Min	0.9	1.1	1.3	1.4
	NMIP/DLEM Max	2.6	3.1	3.4	3.8
Statistical model plus DLEM	SRNM/DLEM	1.3	1.6	1.9	2.1
Inventories	EDGAR v4.3.2	1.3	1.5	1.7	1.9
	GAINS	1.5	1.6	1.7	1.9
	FAOSTAT	1.2	1.5	1.7	1.9
Mean		1.5	1.8	2.0	2.3
Min		0.9	1.1	1.3	1.4
Max		2.6	3.1	3.4	3.8

Supplementary Table 2 N_2O emissions from global total area under permanent meadows and pasture, due to manure N deposition (left on pasture) based on EDGAR v4.3.2, FAOSTAT, and GAINS estimates. Unit: Tg N yr^{-1}

Data sources	1980s	1990s	2000s	2007-2016
EDGAR v4.3.2	1.0	1.1	1.2	1.3
GAINS	0.7	0.7	0.8	0.9
FAOSTAT	1.0	1.1	1.2	1.3
Mean	0.9	1.0	1.1	1.2
Min	0.7	0.7	0.8	0.9
Max	1.0	1.1	1.2	1.3

Supplementary Table 3 N_2O emissions due to global manure management based on multiple bottom-up approaches. Unit: Tg N yr^{-1}

Data sources	1980s	1990s	2000s	2007-2016
EDGAR v4.3.2	0.2	0.2	0.2	0.2
GAINS	0.4	0.4	0.5	0.5
FAOSTAT	0.2	0.2	0.2	0.2
Mean	0.3	0.3	0.3	0.3
Min	0.2	0.2	0.2	0.2
Max	0.4	0.4	0.5	0.5

Supplementary Table 4 Aquaculture N_2O emissions based on multiple sources. Unit: Tg N yr^{-1}

Data sources	Emission factor (%)	1980s	1990s	2000s	2007-2016*
Hu et al.[116]	1.8	N/A	N/A	N/A	0.1
MacLeod et al.[117]	1.8	N/A	N/A	N/A	0.1
Bouwman et al.	1.8	0.01	0.03	0.1	0.1
Bouwman et al._Min	0.5	0.00	0.01	0.02	0.02
Bouwman et al._Max	5.0	0.03	0.1	0.2	0.2

* Estimates in Hu et al.[116] and Macleod et al.[117] were in 2009 and 2013, respectively. N/A represents data are not available.

Supplementary Table 5 Anthropogenic N_2O emissions from the global inland waters based on process-based models. Unit: Tg N yr^{-1}

Data sources/sectors	1980s	1990s	2000s	2007-2016
River_DLEM	0.2	0.2	0.2	0.2
River_Maavara	0.03	0.03	0.03	0.03
River_Mean	0.1	0.1	0.1	0.1
Resevoirs_DLEM	0.05	0.05	0.05	0.05
Resevoirs_Maavara	0.03	0.03	0.03	0.03
Resevoirs_Mean	0.04	0.04	0.04	0.04
Estuaries_Maavara	0.1	0.1	0.1	0.1
Lake_Lauerwald	0.02	0.02	0.02	0.02
Blue carbon_Murray	0.1	0.1	0.1	0.1
Total_Mean	0.3	0.3	0.3	0.3
Total_Min	0.2	0.2	0.2	0.2
Total_Max	0.4	0.4	0.4	0.4

Supplementary Table 6 Anthropogenic N_2O emissions from the global inland waters based on multiple bottom-up approaches. Unit: Tg N yr^{-1}

Data sources	1980s	1990s	2000s	2007-2016
FAOSTAT	0.4	0.4	0.5	0.6
GAINS	0.4	0.4	0.5	0.6
EDGAR v4.3.2	0.5	0.5	0.6	0.7
Model-based	0.3	0.3	0.3	0.3
Mean	0.4	0.4	0.4	0.5
Min	0.2	0.2	0.2	0.2
Max	0.5	0.5	0.6	0.7

Supplementary Table 7 Natural N_2O emissions from the global inland waters based on process-based models. Unit: Tg N yr^{-1}

Data sources/sectors	1980s	1990s	2000s	2007-2016
River_DLEM	0.1	0.1	0.1	0.1
River_Maavara	0.02	0.02	0.02	0.02
River_Mean	0.04	0.04	0.04	0.04
Resevoirs_DLEM	0.04	0.04	0.04	0.04
Resevoirs_Maavara	0.03	0.03	0.03	0.03
Resevoirs_Mean	0.03	0.03	0.03	0.03
Estuaries_Maavara	0.05	0.05	0.05	0.05
Lake_Lauerwald	0.02	0.02	0.02	0.02
Blue carbon_Murray	0.2	0.2	0.2	0.2
Total_Mean	0.3	0.3	0.3	0.3
Total_Min	0.3	0.3	0.3	0.3
Total_Max	0.4	0.4	0.4	0.4

Supplementary Table 8 Nitrous oxide emissions due to atmospheric N deposition on land based on multiple bottom-up approaches. Unit: Tg N yr^{-1}

Data sources	1980s	1990s	2000s	2007-2016
EDGAR v4.3.2	0.3	0.3	0.3	0.4
FAOSTAT	0.3	0.3	0.3	0.4
GAINS	0.3	0.3	0.3	0.4
FAOSTAT/EDGAR v4.3.2	0.6	0.6	0.7	0.8
GAINS/EDGAR v4.3.2	0.6	0.6	0.7	0.7
NMIP_Mean	0.6	0.7	0.8	0.8
NMIP_Min	0.3	0.4	0.4	0.4
NMIP_Max	1.2	1.4	1.3	1.4
Mean	0.6	0.7	0.7	0.8
Min	0.3	0.4	0.4	0.4
Max	1.2	1.4	1.3	1.4

Supplementary Table 9 Global N_2O emissions from waste and waste water based on EDGAR v4.3.2 and GAINS estimates. Unit: Tg N yr^{-1}

Data sources	1980s	1990s	2000s	2007-2016
EDGAR v4.3.2	0.1	0.2	0.2	0.2
GAINS	0.3	0.4	0.4	0.5
Mean	0.2	0.3	0.3	0.3
Min	0.1	0.2	0.2	0.2
Max	0.3	0.4	0.4	0.5

Supplementary Table 10 Global N_2O emissions from fossil fuel and industry based on multiple bottom-up approaches. Unit: Tg N yr^{-1}

Data sources	Sectors	1980s	1990s	2000s	2007-2016
EDGAR v4.3.2	Energy	0.1	0.1	0.1	0.2
	Transportation	0.2	0.2	0.2	0.2
	Others_residential	0.1	0.2	0.2	0.2
	Industry	0.7	0.5	0.5	0.5
GAINS	Energy	0.3	0.4	0.5	0.5
	Industry	0.5	0.5	0.4	0.3
	Mean	0.9	0.9	0.9	1.0
	Min	0.8	0.9	0.8	0.8
	Max	1.1	1.0	1.0	1.1

Supplementary Table 11 Global N_2O emissions from biomass burning based on multiple bottom-up approaches. Unit: Tg N yr^{-1}

Fire categories	Data sources	1980s	1990s	2000s	2007-2016
Crop residues and savannas	GFED4s		0.4	0.4	0.4
	FAOSTAT		0.4	0.4	0.3
	DLEM	0.3	0.3	0.3	0.4
	Mean	0.3	0.4	0.4	0.4
Tropical forests and Deforestation*	GFED4s		0.1	0.1	0.1
	FAOSTAT		0.1	0.1	0.1
	DLEM	0.2	0.2	0.2	0.2
	Mean	0.2	0.1	0.1	0.1
Peatland	GFED4s		0.04	0.01	0.01
	FAOSTAT		0.1	0.1	0.1
	DLEM	0.04	0.05	0.02	0.02
	Mean	0.04	0.06	0.04	0.04
Boreal and temperate forests	GFED4s		0.1	0.1	0.1
	FAOSTAT		0.1	0.1	0.1
	DLEM	0.1	0.1	0.1	0.1
	Mean	0.1	0.1	0.1	0.1
Total_Mean		0.7	0.7	0.6	0.6
Total_Min		0.7	0.5	0.4	0.5
Total_Max		0.7	0.9	0.8	0.8

* DLEM estimates represent burning of tropical forests that are caused by natural and deforestation fires.

Supplementary Table 12 Global oceanic N_2O emissions based on multiple models. Unit: Tg N yr^{-1}

Model	1980s	1990s	2000s	2007-2016
Bern-3D	4.4	4.4	4.3	4.3
NEMOv3.6-PISCESv2-gas	3.3	3.2	3.3	3.4
NEMO-PlankTOM10	3.0	2.8	2.7	2.5
UVic2.9	3.3	3.2	3.2	3.1
NEMO-PISCES 3.2	4.0	3.9	3.9	3.8
Mean	3.6	3.5	3.5	3.4
Min	3.0	2.8	2.7	2.5
Max	4.4	4.4	4.3	4.3

Supplementary Table 13 Global N_2O emissions based on multiple top-down approaches. Unit: Tg N yr^{-1}

Name	Category	2000s	2007-2016
INVICAT	Land	9.7	10.6
	Ocean	7.2	7.1
	Total	16.9	17.7
PyVAR-1	Land	9.4	10.6
	Ocean	6.4	6.4
	Total	15.8	17.0
PyVAR-2	Land	11.8	12.7
	Ocean	4.0	4.3
	Total	15.8	17.0
MIROC4-ACTM	Land	12.5	13.8
	Ocean	3.1	3.4
	Total	15.7	17.1
GEOSChem	Land	10.6	11.3
	Ocean	4.5	4.6
	Total	15.1	15.9
Mean	Land	10.8	11.8
	Ocean	5.1	5.1
	Total	15.9	16.9
Min	Land	9.4	10.6
	Ocean	3.1	3.4
	Total	15.1	15.9
Max	Land	12.5	13.8
	Ocean	7.2	7.1
	Total	16.9	17.7

Supplementary Table 14 Comparison of terminologies used in this study and previous reports.

GCP Terminology (in this study)		IPCC AR5 (IPCC, 2013)	National GHG inventories (used by UNFCCC according to IPCC, 2006 and IPCC, 2019)	UNFCCC / IPCC 2006 Source sector
Anthropogenic sources				
Direct emissions of N additions in the agricultural sector (Agriculture)	Direct soil emissions (mineral N and manure fertilization, cultivation of organic soils, and crop residue returns)	Agriculture	Direct N_2O emissions from managed soils (except due to grazing animals)	3Da without 3Da3
	Manure left on pasture		Urine and dung deposited by grazing animals	3Da3
	Manure management		Manure management	3B
	Aquaculture	---	---	---
Other direct anthropogenic sources	Fossil fuel and industry	Fossil fuel combustion and industrial processes	Energy and industrial processes	1, 2
	Waste and waste water	Human excreta	Waste	5
	Biomass burning (from crop residue, grassland, shrubland and savannas; peat fires, tropical forests, boreal forests, and temperate forests)	Biomass and biofuel burning	Prescribed burning of savannas, field burning of agricultural residues	3E, 3F
Indirect emissions from anthropogenic N additions	Inland and coastal waters (rivers, lakes, reservoirs, estuaries, and coastal zones)	Rivers, estuaries, coastal zones	Indirect emissions due to leaching and runoff	3Db2
	Atmospheric N deposition on land	Atmospheric deposition on land	Indirect emissions due to atmospheric deposition (of agricultural as well as other anthropogenic compounds emitted)	part of 3Db1
	Atmospheric N deposition on ocean	Atmospheric deposition on ocean		part of 3Db1
Perturbed fluxes from climate/CO_2/land cover change	CO_2 effect	---	---	---
	Climate effect	---	---	---
	Post-deforestation pulse effect	---	---	---
	Long-term effect of reduced mature forest area	---	---	---
Natural sources and sinks				
Natural soils baseline		Soils under natural vegetation	---	---
Ocean baseline		Oceans	---	---
Natural (rivers, lakes, reservoirs, estuaries, and coastal upwelling)		---	---	---
Lightning and atmospheric production		Lightning	---	---
		Atmospheric chemistry	---	---
Soil/wetland surface sink		Surface sink	---	---

Supplementary Table 15 Comparison of the global N_2O budget in this study with the IPCC AR5.

	This study (2007–2016)	IPCC AR5 (2006/2011)
Bottom-up budget		
Anthropogenic Sources		
Fossil fuel combustion and industry	1.0 (0.8–1.1)	0.7 (0.2–1.8)
Agriculture (incl. Aquaculture)	3.8 (2.5–5.8)	4.1 (1.7–4.8)
Biomass and biofuel burning	0.6 (0.5–0.8)	0.7 (0.2–1.0)
Wastewater	0.3 (0.2–0.5)	0.2 (0.1–0.3)
Rivers, estuaries, and coastal zones	0.5 (0.2–0.7)	0.6 (0.1–2.9)
Atmospheric N deposition on ocean	0.1 (0.1–0.2)	0.2 (0.1–0.4)
Atmospheric N deposition on land	0.8 (0.4–1.4)	0.4 (0.3–0.9)
Other indirect effects from CO_2, climate and land-use change	0.2 (-0.6–1.1)	
Total Anthropogenic	**7.3 (4.2–11.4)**	**6.9 (2.7–12.1)**
Natural Sources and Sinks		
Rivers, estuaries, and coastal zones	0.3 (0.3–0.4)	
Oceans	3.4 (2.5–4.3)	3.8 (1.8–9.4)
Soils under natural vegetation	5.6 (4.9–6.5)	6.6 (3.3–9.0)
Atmospheric chemistry	0.4 (0.2–1.2)	0.6 (0.3–1.2)
Surface sink	-0.01 (0– -0.3)	-0.01 (0– -1)
Total natural	**9.7 (8.0–12.0)**	**11.0 (5.4–18.6)**
Total bottom-up source	**17.0 (12.2–23.5)**	**17.9 (8.1–30.7)**
Observed growth rate	**4.3 (3.8–4.8)**	**3.6 (3.5–3.8)**
Tropospheric sink	**0.1 (0.1–0.2)**	
Stratospheric sink∗	**13.4 (12.3–14.4)**	**14.3 (4.3–28.7)**
Atmospheric inversion		
Atmospheric loss	12.4 (11.7–13.3)	11.9 (11.0–12.8)
Total source	16.9 (15.9–17.7)	15.8 (14.8–16.8)

Note: ∗ Calculated from satellite observations combined with simple photolysis models in our study.

Supplementary Table 16 Simulation experiments in the NMIP (Tian et al.[1,17])

	CLIM	CO_2	LCC	NDEP	NFER	MANN
SE0	1901-1920*	1860	1860	1860	1860	1860
SE1	1901-2016	1860-2016	1860-2016	1860-2016	1860-2016	1860-2016
SE2	1901-2016	1860-2016	1860-2016	1860-2016	1860-2016	1860
SE3	1901-2016	1860-2016	1860-2016	1860-2016	1860	1860
SE4	1901-2016	1860-2016	1860-2016	1860	1860	1860
SE5	1901-2016	1860-2016	1860	1860	1860	1860
SE6	1901-2016	1860	1860	1860	1860	1860

Note: *CLIM: climate condition; CO_2: atmospheric CO_2 concentration; LCC: land cover change; NDEP: atmospheric N deposition; NFER: mineral N fertilizer use; and MANN: manure N use in cropland. SE0: baseline and control run with repeated climate forcing from 1901-1920; SE1: CLIM+CO_2+LCLU+NDEP+NFER+MANN; SE2: CLIM+CO_2+LCLU+NDEP+NFER; SE3: CLIM+ CO_2+LCLU+NDEP; SE4: CLIM+ CO_2+LCLU; SE5: CLIM+ CO_2; SE6: CLIM. "1901-1920*" denotes that variable is constant at the level of 20-year average; "1860" denotes that variable is constant at the level of 1860; and "1860-2016" denotes that variable changes with time over the study period.*

Supplementary Table 17 Information of NMIP models using in this study

Model	Contact	Affiliation	Publication
DLEM	Hanqin Tian	Auburn University	Tian et al.[18], Xu et al.[19]
LPX-Bern	Sebastian Lienert/ Fortunat Joos	University of Bern, Switzerland	Stocker et al.[20], Xu-Ri & Prentice[21]
O-CN	Sönke Zaehle	Max Planck Institute for Biogeochemistry	Zaehle et al.[22]
ORCHIDEE	Nicolas Vuichard	IPSL – LSCE, France	Goll et al.[23]
ORCHIDEE-CNP	Jinfeng Chang/ Daniel Goll	IPSL – LSCE, France	
VISIT	Akihiko Ito	National Institute for Environmental Studies, Japan	Inatomi et al.[24], Ito et al.[25]

Supplementary Table 18 Summary of models in ocean N_2O inter-comparison

Group	Model	Native resolution (Lon × Lat × Depth)	Publication
U. Bern	Bern-3D	9° × 4.5° × 32 levels	Battaglia and Joos[3]
CNRM	NEMOv3.6-PISCESv2-gas	1° × 1° × 75 levels	Berthet et al.[4]
UEA	NEMO-PlankTOM10	2° × (0.5°–2°) × 30 levels	Buitenhuis et al.[5]
GEOMAR	UVic2.9	3.6° × 1.8° × 19 levels	Landolfi et al.[6]
IPSL	NEMO-PISCES 3.2	2° × (0.5°–2°) × 30 levels	Martinez-Rey et al.[7]

Supplementary Table 19 Overview of the inversion frameworks that are included in the global N_2O budget.

Name	ACTM	Method	Resolution of state vector	ACTM horizontal resolution	ACTM vertical levels	Ocean prior
INVICAT	TOMCAT	4D-Var	5.625°×5.625°	5.625°×5.625°	60	1 (high)
PyVAR-1	LMDz5	4D-Var	3.75°×1.875°	3.75°×1.875°	39	1 (high)
PyVAR-2	LMDz5					2 (low)
MIROC4-ACTM	MIROC4-ACTM	Bayesian analytical	84 regions	2.8°×2.8°	67	3 (low)
GEOSChem	GEOSChem	4D-Var	5°×4°	5°×4°	47	2 (low)

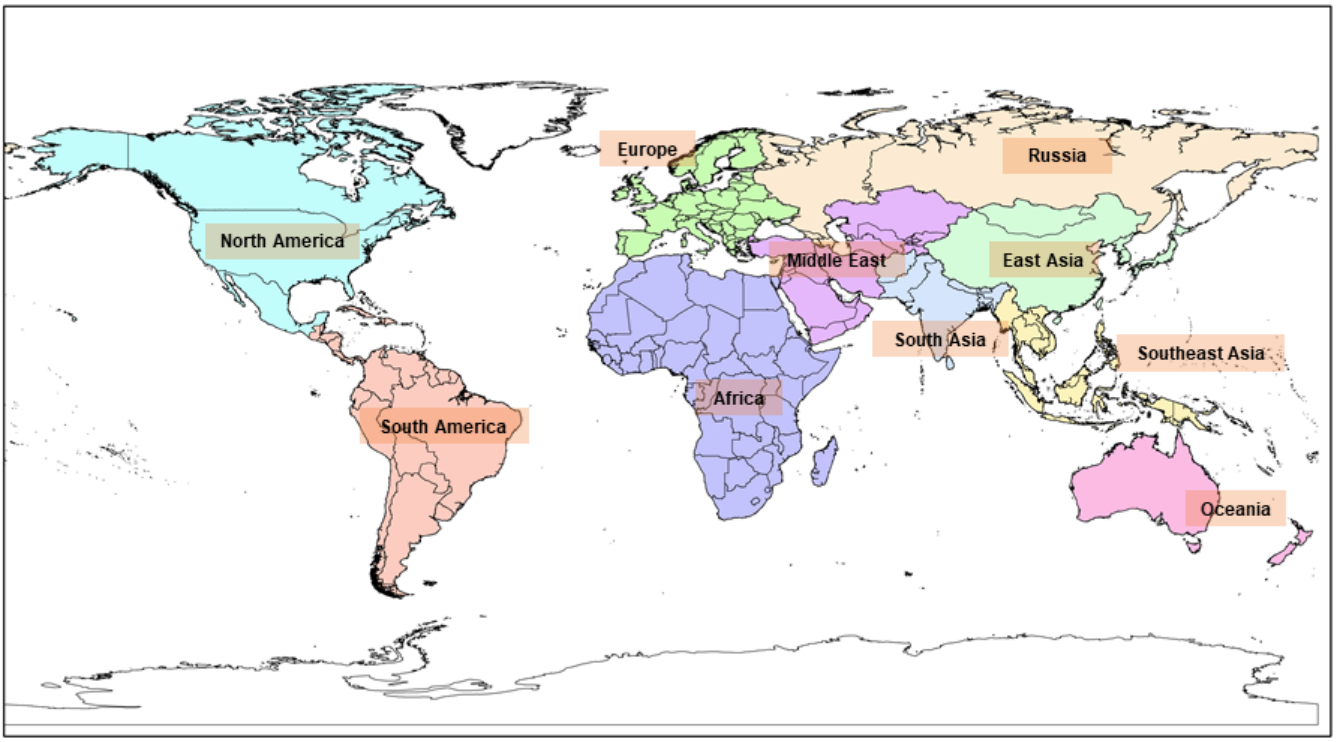

Supplementary Fig. 1 Spatial distribution of ten study regions across the globe.

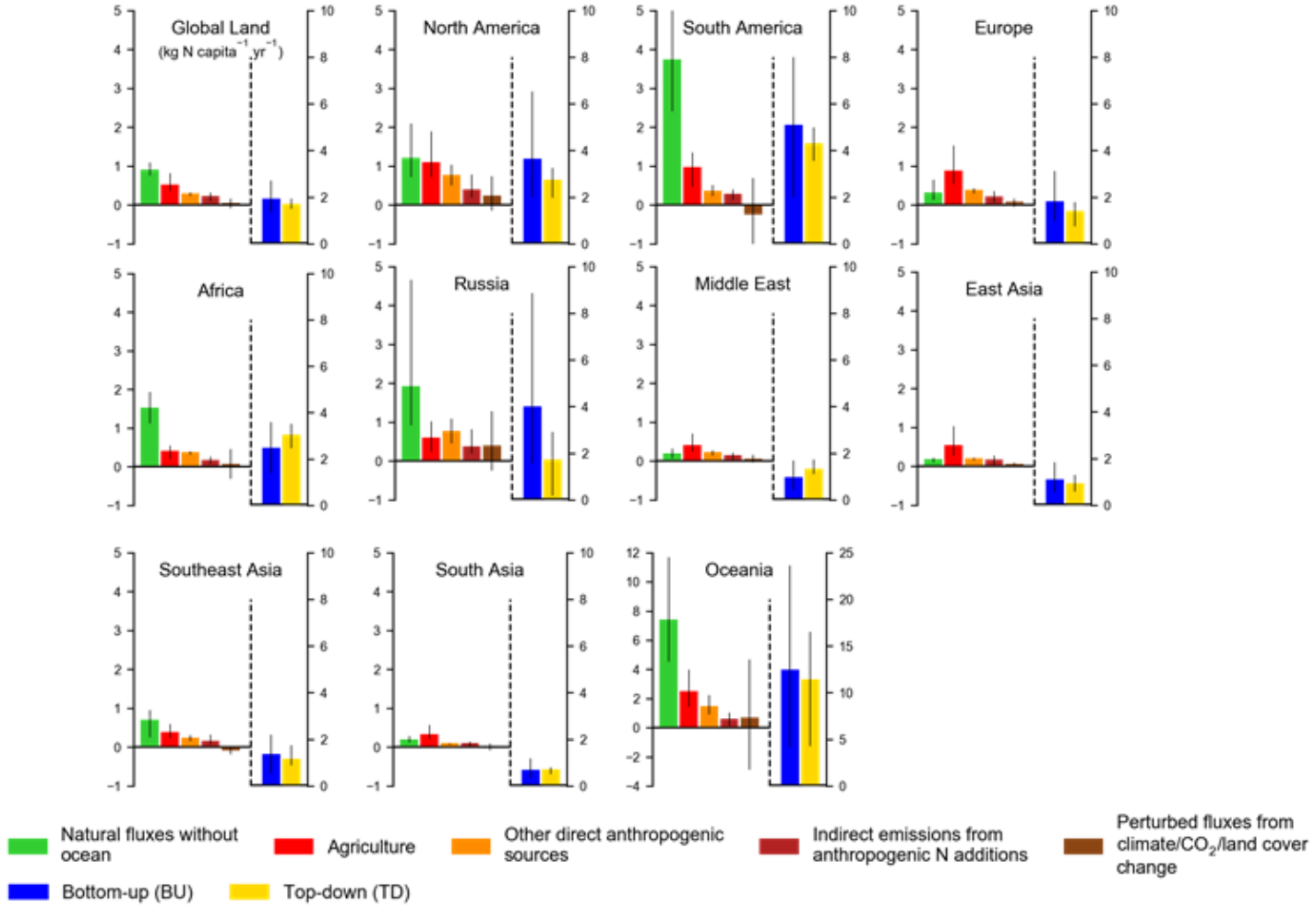

Supplementary Fig. 2 Per capita N_2O emission (kg N capita^{-1} yr^{-1}) during 2007–2016. Annual population was obtained from FAOSTAT[115] (http://www.fao.org/faostat/en/#data/OA).